Active upper-limb prosthesis for swimming

by

Vasylysa Korovkina

A thesis
presented to the University of Waterloo
in fulfillment of the
thesis requirement for the degree of
Master of Applied Since
in
System Design Engineering

Waterloo, Ontario, Canada, 2025

© Vasylysa Korovkina 2025

Author's Declaration

I hereby declare that I am the sole author of this thesis. This is a true copy of the thesis, including any required final revisions, as accepted by my examiners.

I understand that my thesis may be made electronically available to the public.

Abstract

Swimming presents unique challenges for individuals with upper-limb absence, as it requires complex coordination, symmetric propulsion, and control of body balance. Despite these demands, swimming also offers significant rehabilitative benefits, promoting muscle engagement, joint mobility, and cardiovascular health. However, current upper-limb prostheses rarely address the specific requirements of swimming, and most available devices remain passive or non-functional in aquatic environments.

This thesis proposes a novel design for a swimming-specific forearm prosthesis that actively adjusts wrist orientation in response to the swimmer's forearm motion. By segmenting the freestyle stroke into distinct phases—entry, catch, pull, push, and recovery—the control system simplifies the dynamic task into manageable sub-problems. Each phase is associated with a predefined wrist rotation, which simplifies control by reducing the continuous motion into a set of discrete, easily manageable movements. The phase recognition is performed using an inertial measurement unit (IMU), which monitors arm motion and triggers appropriate commands to the servo motor embedded in the prosthesis.

A prototype was developed to demonstrate this concept. The device includes a custom 3D-printed forearm structure that houses all electronic components—IMU, servo motor, controller, and battery—and uses a belt-pulley mechanism to transmit motion. Although the prototype is not yet suitable for use in water, it effectively demonstrates the feasibility of phase-based control for dynamic tasks such as swimming. The design emphasizes modularity, simplicity, and the potential for future development into a fully water-resistant system suitable for rehabilitation, recreational use, or part of training for competitive para-swimmers.

Acknowledgements

I would like to express my sincere gratitude to all the people who made this thesis possible.

First and foremost, I would like to thank my supervisor, Professor John McPhee, for his continuous support, encouragement, and invaluable guidance throughout my research. I am also deeply grateful to the members of my thesis committee, Professor James Tung and Professor Mihaela Vlasea, for their time, feedback, and thoughtful suggestions that helped shape this work. I extend my thanks to all faculty members who have taught, advised, and inspired me throughout my academic journey. I am also thankful to the instructors I had the opportunity to work with as a teaching assistant, and to the students who challenged me to grow.

Special thanks go to the students and researchers of the Motion Research Group (MoRG) for their insightful discussions, helpful suggestions, and day-to-day support throughout my time in the lab.

I am also deeply thankful to the organizers of the Summer Program for Students at Risk from Ukraine, whose support allowed me to come to Waterloo for an internship and ultimately begin my Master's studies here. Their encouragement and belief in my potential made this path possible.

On a more personal note, I would like to thank my swimming coach, Vadym Rabotiuk, for teaching me how to swim, for patiently answering all my technical questions during training and research, and for his courage in defending our homeland. My deepest gratitude goes to my husband, Volodymyr Korovkin, whose care, patience, and unwavering support helped me navigate this journey. I am grateful to my friends, who kept me grounded and uplifted during this transformative period of my life, and to my parents, whose love and support reached me even from thousands of kilometers away.

This thesis would not have been possible without each of you. Thank you!

Dedication

To all the brave people who defend and support Ukraine, and to the warriors and civilians who, in the face of life-changing injuries, continue to live with dignity, purpose, and the power to inspire others.

Table of Contents

Author's Declaration ii

Abstract iii

Acknowledgements iv

Dedication v

List of Figures ix

1 Introduction 1

1.1 Motivation and Goals 1

1.2 Contribution and Document Structure 4

2 Background and Literature Review 5

2.1 Physiological and Psychological Effects of Amputation 5

2.2 Modern Prostheses 7

2.2.1 Prostheses Control with IMU 9

2.2.2 Prostheses for Swimming 10

2.3 Swimming as a Rehabilitation Practice 10

2.3.1 Physiological Effects 10

2.3.2 Psychological Effects 12

2.4 Biomechanics of Swimming . . . 13
2.5 Swimming with Limb Absence . . . 16

3 Kinematics Analysis **18**
3.1 Swimming Kinematics Dataset . . . 18
3.2 Kinematic Data from Dry-Land Swimming Trials . . . 20
3.3 Data Processing and Stroke Phase Segmentation . . . 23

4 Design **27**
4.1 System Requirements . . . 27
4.2 Mechanical Design . . . 29
4.2.1 CAD Models . . . 29
4.2.2 Hand Shape . . . 30
4.2.3 Wrist Joint Mechanism . . . 32
4.2.4 Forearm . . . 35
4.3 Control System Design . . . 40
4.3.1 Swimming Phase Detection . . . 41
4.3.2 Kinematic Mapping . . . 42
4.3.3 Implementation Details . . . 43
4.4 Electrical Design . . . 44

5 Prototyping **48**
5.1 3D Printing . . . 48
5.2 Assembling Process . . . 49
5.3 Testing . . . 54

6 Conclusions and Future Research **59**
6.1 Contributions . . . 59
6.2 Limitations . . . 60
6.3 Opportunities for Future Work . . . 61

References 63

APPENDICES 70

A Bill of Materials (BOM) for the swimming prosthesis prototype 71

List of Figures

1.1 Examples of commercially available water sport terminal devices [1]. 3

2.1 Schematic of the biological wrist-hand complex showing 27 degrees of freedom (DoF). 8

2.2 Arm stroke phases in front-crawl (classification proposed by Chollet et al.,[2]). 14

2.3 Orientation of the IMU axes used in this study. The orange box indicates the IMU placement. 15

3.1 Sample kinematic data from one swim trial showing wrist joint angle (sagittal plane) and elbow joint angular velocity. 20

3.2 Placement of Xsens MVN Awinda IMUs used for full-body motion capture and axis of segments (Modified from [3]). 21

3.3 Experimental setup for dry-land swimming simulation using the Xsens MVN Awinda motion capture system with global axes at the University of Waterloo. 22

3.4 Flexion/extension of the wrist (top plot) and corresponding forearm mediolateral angular velocity measured by an IMU (bottom plot) over four consecutive strokes. Vertical dashed lines denote stroke phase transitions: red for the end of the catch, green for the end of the pull, and blue for the end of the push. 23

3.5 Mean kinematic profiles of the right-hand wrist during a representative front crawl stroke. (A) Angular velocity of the forearm around the Y-axis relative to the pelvis, with phase segmentation. (B) Angular velocity of the forearm around the Z-axis relative to the pelvis, with phase segmentation. (C) Wrist flexion-extension angle, with phase segmentation. The shaded areas represent the standard deviation across trials. 25

4.1 Concept art of the proposed prototype. 29
4.2 CAD rendering of the prosthetic hand design (three perspectives). 32
4.3 M10 hex bolt repurposed as a wrist shaft. 34
4.4 Wrist joint CAD model. The dashed line indicates the wrist joint axis. (1) Hand part, (2) Wrist part, (3) Pulley. 35
4.5 Forearm CAD model showing external compartments in three views. Key components are indicated as follows: (1) enclosure for the servo motor, (2) enclosure for electronics. 36
4.6 Servo motor enclosure with custom tensioning mechanism. Key components: (1) screws with washers that clamp the motor position, (2) vertical screw providing additional stabilization, (3) slotted mounting rails that allow the motor to slide during adjustment. 37
4.7 Forearm CAD model in two views. Key components are indicated as follows: (1) main housing, (2) side lid, (3) button lid.The dashed line represents the wrist joint axis. 39
4.8 Block diagram of phase-based wrist control. 40
4.9 Phase segmentation based on the proposed control algorithm using forearm angular velocity (ω_Y and ω_Z). (A) Angular velocity around the Y-axis relative to the pelvis. (B) Angular velocity around the Z-axis relative to the pelvis. 42
4.10 Electrical block diagram of the control system. 45
4.11 Assembled soldered electrical circuit. 47

5.1 Prototype: three views illustrating the range of motion. 49
5.2 Assembled CAD model shown from two perspectives. 51
5.3 Internal view of the prosthesis. Key components are indicated as follows: (1) servo motor, (2) 3.7 V battery, (3) 12 V battery, (4) belt of the belt drive, (5) small pulley, (6) large pulley. 53
5.4 Annotated video of the prototype in Tracker, showing magenta axes and four tracked points with their motion traces. 56
5.5 Comparison of mean wrist flexion–extension between dry-land trials (Section 3.2) and the prototype: (A) Dry-land motion with labeled stroke phases; shaded area represents ±1 standard deviation. (B) Prototype motion with labeled stroke phases; shaded area represents ±1 standard deviation. . . . 57

5.6 Phase portrait of the prosthetic prototype wrist controller: mean forearm angular velocity (Y axis) vs. mean wrist flexion–extension angle (X axis) with annotated stroke phases 58

Chapter 1

Introduction

Individuals who undergo hand amputations face lifelong challenges, navigating everyday activities with reduced upper-limb mobility and adapting to the absence of the limb. In this context, prosthetic technologies play a crucial role, offering biomechatronic solutions that aim to restore some degree of lost functionality and significantly improve quality of life. Beyond facilitating daily activities, prostheses contribute to physical rehabilitation after amputation by reducing complications such as phantom limb pain (PLP) and compensatory musculoskeletal strain.

1.1 Motivation and Goals

Armed conflicts, industrial accidents, and natural disasters remain among the leading causes of traumatic amputations worldwide. While the majority of published epidemiological data to date originate from earlier conflicts such as those in Iraq and Afghanistan, where explosive devices accounted for the overwhelming majority of major limb losses, modern warfare demonstrates an equally — if not more — severe impact [4, 5]. The ongoing full-scale invasion of Ukraine by the russian federation has resulted in a large and rapidly growing number of upper- and lower-limb amputations, affecting not only military personnel but also civilians, including children. Unlike many previous conflicts, this war is characterized by deliberate attacks on residential areas and civilian infrastructure, leading to a high proportion of complex blast and crush injuries [6, 7]. Although comprehensive, peer-reviewed statistical analyses of these injuries in Ukraine are still limited due to the ongoing nature of the conflict, the available reports and medical observations already indicate

a significant and long-term public health challenge that will require extensive rehabilitation resources for decades to come.

Among the most severe mechanisms of injury in such contexts is crush syndrome — a life-threatening condition that occurs when a limb is trapped under heavy debris, causing prolonged ischemia, muscle necrosis, and systemic metabolic complications. In many cases, delayed extrication or inadequate blood flow restoration necessitates urgent amputation to prevent fatal outcomes. Alongside blast trauma, crush syndrome has become a frequent cause of limb loss in contemporary war zones, particularly where civilians are trapped under collapsed buildings following targeted shelling of urban areas.

Traumatic upper-limb amputation (TULA) represents a severe and complex injury with profound consequences. Beyond the immediate functional loss, such as the inability to perform bimanual tasks, reduced dexterity, and limitations in activities of daily living, individuals frequently experience long-term psychological challenges, including depression, anxiety, post-traumatic stress disorder (PTSD), and pathological grief (PG), with reported prevalence rates of depression ranging from 20–63% and anxiety from 25–57% [8, 9, 10]. Such conditions are often compounded by PLP, which can become chronic and disrupt cognitive functioning, emotional wellbeing, sleep quality, and social interactions [11]. Physiological consequences, such as muscle atrophy, altered metabolism, and compensatory movement patterns, further impair recovery and prosthetic control [12]. These combined mental and physical burdens highlight the necessity for multidisciplinary rehabilitation strategies that address both psychological health and functional restoration from the earliest stages of recovery. Standard rehabilitation in such cases involves integrated mental health support alongside physical training aimed at stress reduction, strength development, and muscle mass preservation.

Swimming is widely recognized for its rehabilitative benefits, offering low-impact, whole-body exercise that supports cardiovascular health, muscular balance, and mental well-being [13]. However, individuals with upper-limb amputations face substantial limitations when engaging in this activity, as commercially available swimming-specific prostheses remain scarce and often lack functional design.

The absence of one arm during swimming creates biomechanical asymmetry, leading to unbalanced stroke patterns. Over time, this may result in overuse injuries, such as shoulder impingement, neck strain, or mechanical low back pain [14], adding to the existing musculoskeletal imbalance caused by amputation. While swimming is often recommended for lower-limb amputees as a form of cardiovascular exercise and rehabilitation [15], upper-limb amputees remain underserved due to limited device availability and lack of integration between biomechanics and assistive technology.

On the current market, only a few swimming-specific prosthetic options are available, as illustrated in Figure 1.1. These devices are typically passive, offering basic stroke support without generating additional propulsion [16]. Their rigid construction and lack of hydrodynamic optimization limit adaptability across different swimming styles and reduce overall efficiency in the water. Moreover, swimmers with upper-limb amputations often face increased compensatory shoulder torque to maintain stroke symmetry, which can result in muscular overuse or secondary injuries over time [14]. While some designs attempt to achieve neutral buoyancy to minimize drag and reduce compensatory motion [17], current solutions do not address the absence of dynamic, phase-specific actuation, leaving a significant gap in functional performance.



Figure 1.1: Examples of commercially available water sport terminal devices [1].

Importantly, although prosthesis use is prohibited in most forms of competitive swimming, the development of such technology for recreational, therapeutic, or training purposes is of great value [15, 18].

1.2 Contribution and Document Structure

To the best of the author's knowledge, there are currently no upper-limb prosthetic systems specifically designed for swimming that incorporate active wrist actuation and adapt the wrist angle dynamically based on stroke phase. This thesis proposes a novel system that integrates biomechanical analysis and control-based actuation to address this gap. The development and evaluation of such a system contributes to the fields of aquatic rehabilitation and adaptive prosthetics for sport and recreational use. In this work, the primary focus was placed on the front crawl, as it is one of the most fundamental and widely-practiced swimming techniques, and its implementation requires relatively limited variation in hand movements.

This thesis is organized as follows:

Chapter 2 presents a literature review covering the physiological and psychological effects of amputation, upper-limb prostheses for swimming, IMU-based control strategies, and the biomechanics of swimming with limb absence.

Chapter 3 describes the analysis of swimming kinematics using both water-based and dry-land motion capture data to inform prosthesis control strategies.

Chapter 4 outlines the design of the proposed prosthetic system, including mechanical structure, control logic, and electrical integration.

Chapter 5 details the prototyping process using 3D printing and presents the initial testing and assembly outcomes.

Chapter 6 concludes the thesis with a summary of key findings, discussion of limitations, and suggestions for future work.

Chapter 2

Background and Literature Review

2.1 Physiological and Psychological Effects of Amputation

Traumatic upper-limb amputation (TULA) produces a complex set of physiological and psychological consequences that deeply influence patients' quality of life and rehabilitation outcomes. Alongside obvious functional impairments, psychological distress is highly prevalent and may persist for years after the initial trauma. Depression, anxiety, post-traumatic stress disorder (PTSD), and pathological grief (PG) are among the most common mental health conditions observed in this population [9, 8, 10, 19]. PG, defined as a persistent inability to adapt to the loss of a limb, affects more than one-third of individuals after traumatic amputation and is associated with markedly elevated psychological suffering [9].

Several factors increase vulnerability to PG and other disorders: amputations involving the thumb, proximal or multiple-digit loss, absence of attempted revascularization, and a subjective sense of mutilation stemming from both functional and aesthetic impairments [9]. Chronic stump pain can further aggravate psychological burden, highlighting the need for rehabilitation strategies that address mental health alongside physical recovery [9].

Reported prevalence of depression in traumatic amputees ranges from 20–63%, while anxiety rates vary from 25–57%, often peaking soon after injury [8]. Although some improvement may occur over time, many individuals face enduring mental health challenges. Comparative studies with non-amputee trauma patients suggest that grief over limb loss is a unique and substantial contributor to these outcomes [8]. PTSD is also common, particularly in military populations with combat-related upper-extremity amputations, where

prevalence estimates range from 21% to 69%, with co-occurring depression reported in 6–36% of cases [10]. In civilians, similarly high rates have been documented, especially among transradial amputees, who show depression prevalence up to 69% and PTSD rates of 85% [10, 20]. The psychological toll is generally greater for upper-limb amputees compared to those with lower-limb loss, likely due to the greater functional and social importance of the upper extremities [9]. Interestingly, prosthesis use alone does not significantly mitigate PG risk; many patients prioritize cosmetic devices to improve body image over purely functional solutions [9].

From a physiological standpoint, TULA triggers substantial alterations in body composition and metabolism. Muscle atrophy and increased adiposity are frequent, driven by physical inactivity, neurogenic muscle fiber shrinkage, medication effects, and changes in dietary intake [12, 21]. The degree of muscle atrophy in the residual limb correlates with the amputation level, with higher-level amputations producing more severe losses [12]. Even modest reductions in muscle mass can have significant clinical consequences—losses of 5% may impair organ function, while reductions exceeding 20% can result in organ failure and increased mortality risk [12]. These catabolic states also hinder wound healing, limit participation in rehabilitation, and delay functional recovery.

While lean mass diminishes, fat mass often increases. Early after trauma, metabolic responses resemble those seen in critical illness: elevated basal metabolic rate, intense protein catabolism, and hormonal changes driving nutrient redistribution [12]. Energy demands during the inflammatory and wound-healing phases can rise by 30–50%, later returning to baseline as acute recovery ends. However, prolonged rehabilitation or repeated surgeries may perpetuate altered metabolic states, a process that remains poorly understood [12]. Observational studies in amputees—primarily those with nontraumatic, dysvascular etiologies—show weight gain in both unilateral and bilateral cases, with unilateral amputees sometimes experiencing paradoxical increases in lean mass without proportional increases in lean mass percentage. Significant fat accumulation has been observed within the first nine months post-amputation in unilateral patients [12].

Among the most challenging post-amputation complications is PLP, which frequently emerges soon after surgery and may persist chronically. PLP presents with highly variable intensity, frequency, and sensory characteristics, affecting not only physical comfort but also cognitive performance and emotional wellbeing [11]. Patients report difficulties concentrating, heightened irritability, and increased rates of depression, while disrupted sleep and altered social interactions further compound psychological distress [11]. Notably, PLP has been linked to prosthesis discontinuation, especially in cases where shoulder stiffness develops, underscoring its relevance to both physical and mental rehabilitation [22].

Surgical and orthopedic complications also play a role in long-term outcomes. In a retrospective study of combat-related major upper-extremity amputations, 42% of cases required revision surgeries, most often due to deep infections [22]. Nevertheless, functional results following revision were promising: 84% of patients ultimately used prostheses, with post-revision use rising from 19% to 87% [22]. Disability ratings were significantly higher for upper-limb amputees compared to lower-limb amputees (83% vs. 62%), reflecting the more profound impact on daily function [22].

In summary, traumatic upper-limb amputation exerts severe and multifaceted effects on both body and mind. High rates of depression, anxiety, PTSD, and pathological grief underscore the need for integrated psychological support at all rehabilitation stages. Concurrently, muscle atrophy, metabolic changes, phantom limb pain, and surgical complications create persistent physical challenges that can undermine functional recovery. Optimal long-term outcomes require comprehensive, multidisciplinary care that simultaneously addresses physical rehabilitation, mental health, and early identification of risk factors, thereby facilitating better adaptation and reintegration into daily life.

2.2 Modern Prostheses

Prostheses are artificial wearable limbs designed to replace missing extremities, aiming to restore functional capabilities and improve users' quality of life [23]. Typically, a transradial prosthesis consists of a terminal device — usually a prosthetic hand — mounted on a prosthetic wrist. Depending on their mode of operation, these devices are classified as cosmetic (also known as passive), body-powered, or externally powered (active) prostheses [23, 24].

The primary function of powered prosthetic hands and wrists is to replicate essential grasping patterns used in daily activities, such as power grip, precision grip, lateral grip, and index point [22]. These grips vary in frequency of use, influencing the mechanical design and control strategies of prosthetic devices. The biological wrist-hand complex possesses approximately 27 degrees of freedom (DoF; see Figure 2.1). Each of the four fingers has 4 DoF: 3 for flexion and extension, and 1 for abduction and adduction. The thumb is more complex, with 5 DoF, while the wrist itself has 6 DoF, accounting for rotation and translation. This configuration enables a wide range of dexterous tasks [23]. To approximate this complexity, various mechanical designs have been developed, including linkage-based and tendon-driven underactuated finger mechanisms, which allow for efficient and compact actuation [23].

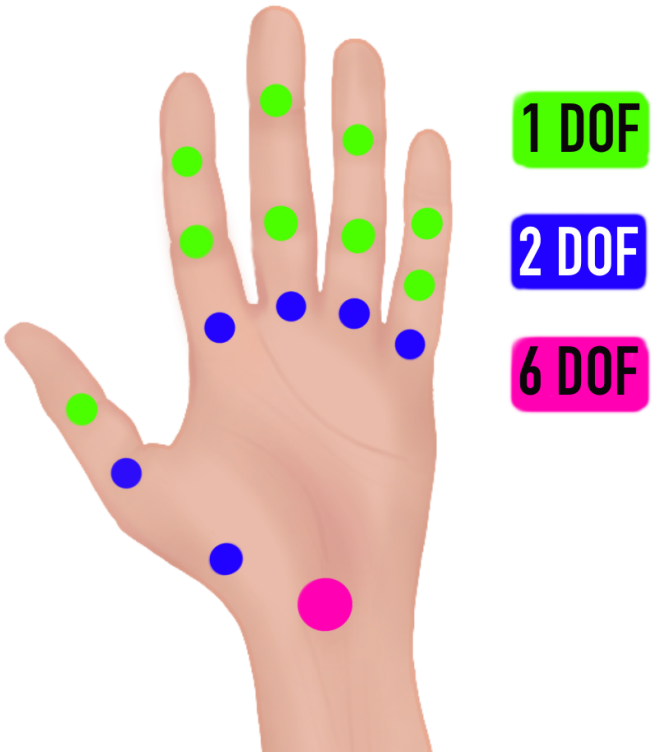


Figure 2.1: Schematic of the biological wrist-hand complex showing 27 degrees of freedom (DoF).

Among modern advances, the myoelectric prosthesis stands out as the most sophisticated, utilizing surface electromyography (EMG) signals from residual limb muscles or the shoulder to infer intended finger and wrist movements [23]. Proportional control schemes enable graded motions after rigorous user training, improving the naturalness of prosthetic use [23]. These devices tend to be heavier, more expensive, and require longer adaptation periods compared to body-powered or cosmetic alternatives [22]. Despite these challenges, myoelectric prostheses are preferred by approximately 66% of transradial amputees [22]. Notably, users of this category report a higher incidence of phantom limb pain and an increased need for neuropathic pain medication [22].

Body-powered prostheses, which use cable and harness systems to actuate terminal devices, offer robust durability and superior sensory feedback through mechanical linkages [22]. In contrast, cosmetic prostheses prioritize lightweight design and minimal intrusion, but provide limited functional utility.

The selection of the number of actuators in prosthetic hands correlates directly with the number of grasping patterns the device is designed to perform, necessitating a trade-off between mechanical complexity, weight, and control intuitiveness [23]. Tendon-based mechanisms allow miniaturization by relocating actuators away from the joints, facilitating compact and lightweight prosthetic hands without compromising functionality [23].

Technological progress in manufacturing has introduced 3D printing as a disruptive approach to prosthetic fabrication. This method enables rapid, cost-effective production and customization, accommodating diverse user anatomies and preferences [25]. Recent developments include 3D-printed soft monolithic robotic hands optimized via finite element analysis (FEM) to enhance manipulation of delicate objects with fewer sensors, outperforming traditional rigid prostheses [25]. Parametric design frameworks allow intuitive adjustment of prosthetic dimensions through graphical interfaces or spreadsheets, offering scalable personalization [25].

Despite these advances, prosthetic devices continue to face substantial challenges including imperfect functional control, limited degrees of freedom, and issues related to size, weight, and aesthetics [23]. Proper prosthetic fitting combined with targeted training remains crucial for maximizing functional outcomes, enabling amputees to more rapidly resume work and daily activities [22]. Moreover, the fabrication process itself—including molding, fitting, and iterative refinements—adds further complexity, as each stage requires careful tailoring to the individual to achieve both comfort and functionality.

In summary, modern prostheses integrate mechanical innovation, sensor technologies, and novel manufacturing techniques to approximate natural limb function. However, ongoing research and development remain essential to address persistent challenges and further improve user acceptance, comfort, and overall quality of life.

2.2.1 Prostheses Control with IMU

Control systems are at the core of functional prosthetics. In lower-limb devices, inertial measurement units (IMUs) are widely used to detect gait phases through gyroscopes and accelerometers, enabling stable, real-time control of repetitive movements [26, 27]. For upper limbs, electromyography (EMG) remains dominant, but combining EMG with IMU data has emerged as a promising approach [28, 29]. This multimodal control allows for faster, more coordinated, and intuitive movements, improving user satisfaction.

Piezoresistive and capacitive accelerometers offer dual-axis measurements with high stability, critical for precise tracking [26]. In aquatic environments, where EMG signals often suffer from noise and reduced reliability, IMUs remain robust [30, 31, 32]. Mapping

IMU data to swimming stroke phases enables adaptive wrist or joint positioning in real time, benefiting both rehabilitation and sport-specific applications.

A hybrid IMU–EMG approach to transradial prosthesis wrist control has shown notable improvements over conventional EMG-only control: able-bodied test participants completed tasks 33% faster, with reduced compensatory torso movement and higher perceived intuitiveness [31]. In these assessments, which included the Compound Rotation Task (CRT) and the Compound Manipulation Task (CMT), participants were required to relocate objects within a set time while alternately changing wrist orientations. They performed sequences of grasps (lateral pinch, cylindrical, spherical) that simulated realistic hand–wrist usage.

2.2.2 Prostheses for Swimming

While land-based prosthetic technology has advanced considerably, swimming-specific devices remain scarce and underdeveloped. Most available solutions are rigid, lack hydrodynamic optimization, and do not adapt to various swimming styles [16]. This creates biomechanical challenges for swimmers with upper-limb amputations, particularly increased compensatory shoulder torque, which can lead to overuse injuries [14].

Neutral buoyancy has been explored as a way to improve comfort and efficiency in water by reducing drag and restoring balance [17]. However, buoyancy alone cannot replicate the dynamic motion of a natural limb. The ideal aquatic prosthesis would combine neutral buoyancy with active or adaptive control, synchronizing with stroke phases to modulate joint angles or stiffness. Such innovations could alleviate strain on the shoulder, enhance rehabilitation, and expand opportunities for competitive and recreational swimming for amputees.

2.3 Swimming as a Rehabilitation Practice

2.3.1 Physiological Effects

Regular swimming induces a range of long-term physiological adaptations with both statistical and clinical significance. Training in an aquatic environment has been shown to improve absolute, relative, and post-intervention relative VO_{2max}, reflecting enhanced aerobic capacity and efficiency of oxygen utilization [13]. Interestingly, no significant differences

have been observed between swimming and running in terms of relative VO_{2max}, indicating that swimming can serve as an equally effective aerobic exercise modality despite its non-weight-bearing nature.

In addition to cardiorespiratory benefits, swimming positively influences pulmonary function through repeated exposure to the respiratory demands of immersion and controlled breathing patterns. Immersion in water imposes a mild hydrostatic compression on the thorax, which increases the resistance to inspiration, thereby strengthening respiratory muscles over time. Post-intervention peak expiratory flow has been reported as significantly greater in the swimming group compared to control groups [13]. Similarly, forced expiratory volume in the first second (FEV_1, % predicted) improved significantly in swimmers compared to participants engaged in low-intensity activity, such as golf. Another study involving female high school students demonstrated significant gains in maximal breathing capacity among swimmers, whereas no measurable changes were observed in the non-swimming control group.

Swimming has also been associated with significant increases in lean body mass. This outcome has been documented in healthy children, adolescents, and adults, as well as in adults with hypertension [13]. The uniform resistance provided by water's viscosity promotes balanced muscular engagement across multiple muscle groups, while buoyancy reduces eccentric loading, allowing for consistent training with minimal joint stress. This combination makes it possible to improve strength and muscular endurance without the injury risks often seen in high-impact sports.

These adaptations extend beyond aerobic fitness and muscle mass. Aquatic exercise, widely regarded as a highly effective form of training, offers reductions in joint pain and improvements in joint mobility due to decreased compressive forces on articular structures. Moreover, it provides an accessible exercise option for individuals unable to participate in weight-bearing land-based activities, enabling them to achieve substantial gains in cardiovascular conditioning. The thermal properties of water—particularly in heated pools—can also promote vasodilation and muscle relaxation, enhancing recovery and comfort during exercise. Supporting this, a study on patients with fibromyalgia found that after a 12-week swimming programme, participants experienced significant reductions in perceived pain and stiffness [33].

Overall, the physiological effects of swimming encompass improvements in cardiovascular endurance, respiratory efficiency, muscle composition, and joint health, achieved through the combined influence of buoyancy, hydrostatic pressure, and water resistance. These features position swimming as a comprehensive exercise modality capable of delivering benefits comparable to high-impact training while minimizing musculoskeletal strain.

2.3.2 Psychological Effects

Mood disorders and anxiety significantly reduce quality of life and overall well-being [34]. Physical activity has increasingly been recognized as an effective non-pharmacological intervention for improving mental health, with aerobic exercise in particular demonstrating consistent benefits [34]. For example, exercise has been recommended as a first-line treatment in the Canadian Clinical Guidelines for emotional therapy [34].

Among different forms of physical activity, aquatic exercise has been shown to have a particularly strong positive impact on psychological health [34, 35]. Water immersion provides a unique environment, where buoyancy, hydrostatic pressure, and water resistance not only reduce joint loading but also induce a calming sensory experience that may help alleviate symptoms of anxiety and depression [34]. Compared to land-based activities, aquatic exercise often produces greater mood-enhancing effects, which can be attributed to both physiological mechanisms and the distinctive sensory input provided by water [34].

Meta-analyses support these findings, showing that aquatic exercise results in statistically significant reductions in symptoms of mental disorders compared to pre-intervention levels [34]. Subgroup analyses further revealed that the most pronounced effects were observed in adults aged 18–64 years, while other age groups demonstrated smaller but still measurable benefits [34]. These results indicate that psychological outcomes depend not only on the exercise itself but also on factors such as age, intensity, and individual health status.

Exercise intensity is considered one of the most critical parameters for mental health improvement. The American College of Sports Medicine classifies heart rate below 64% of maximum as low intensity, 64–76% as moderate, and 77–95% as high intensity [34]. Low-intensity aquatic exercise is associated with relaxation and stress relief, whereas moderate-to-high intensity appears sufficient to trigger neurochemical changes, such as the release of β-endorphins and dopamine, which are strongly linked to mood elevation [34, 33].

Physiological mechanisms provide additional support for the mental health benefits of swimming. Water resistance—more than ten times greater than that of air—requires greater motor cortex activation, potentially stimulating brain regions associated with cognitive and emotional regulation, particularly in older adults [34]. Furthermore, aquatic exercise has been shown to decrease levels of pro-inflammatory cytokines, such as TNF-α and IL-6, which are often associated with mood disorders and psychological distress [34].

When compared to other non-pharmacological interventions, aquatic exercise stands out. For example, a meta-analysis conducted by Song demonstrated that its effect on anxiety reduction was substantially greater than that of land-based aerobic exercise, tradi-

tional Chinese exercise, or meditation [34]. These superior effects may be explained by the tactile feedback of water flowing across the skin, which has been linked to stress reduction and mood improvement [34].

Nevertheless, certain factors can influence these outcomes. For instance, cold-water swimming has shown limited benefits for mental health, likely due to the excessive stress response triggered by low temperatures [34]. Additionally, variability between aquatic exercise types, such as swimming and water aerobics, may contribute to the heterogeneity observed in study results [34].

Systematic reviews further confirm these benefits. Across 23 studies, aquatic exercise was associated with improvements in depression (16 studies), anxiety (8 studies), mood (6 studies), self-esteem (2 studies), and overall psychological well-being (3 studies) [33]. Notably, these findings are not limited to statistical measures: for instance, one case study described a female patient who, after a structured leisure swimming program, was able to discontinue antidepressant medication entirely [33].

Taken together, these findings highlight that aquatic exercise—particularly at low to moderate intensity—offers a unique and highly effective approach to improving mental health. Its combined physiological, neurological, and sensory effects explain why it frequently outperforms land-based exercises in reducing symptoms of depression and anxiety [33]. As such, aquatic exercise should be considered a key element not only for physical rehabilitation but also as a complementary therapy for psychological recovery and improved overall well-being.

2.4 Biomechanics of Swimming

Front crawl swimming is a highly coordinated, cyclical activity involving complex interactions of multiple muscle groups and joints. Propulsion in swimming is predominantly generated by the upper limbs, with the arm stroke in front-crawl contributing about 87–90% of the overall swimming speed [36, 37]. According to [38], the hand alone contributes approximately 67% of the propulsive force produced by the combined hand–forearm unit.

To better understand the mechanics of propulsion in front crawl, the swimming stroke is often divided into a sequence of distinct phases based on the position and motion of the arm throughout the stroke cycle. This segmentation facilitates biomechanical analysis, enabling researchers and coaches to identify key moments of force production, joint loading, and technical efficiency. The classification applied in this work is illustrated in Figure 2.2.

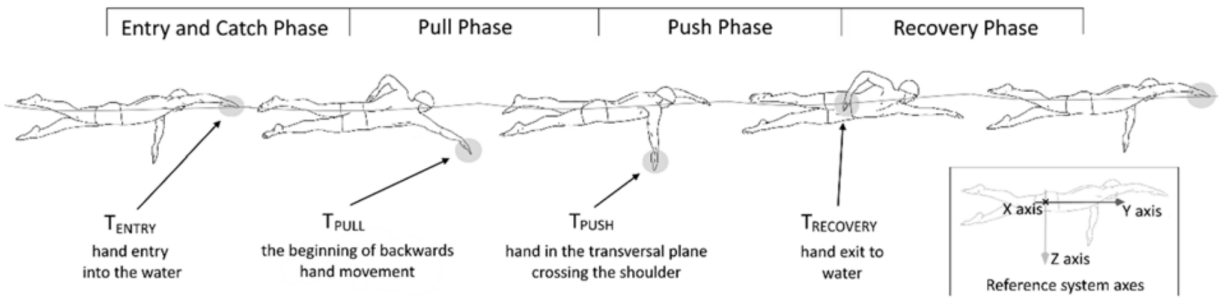


Figure 2.2: Arm stroke phases in front-crawl (classification proposed by Chollet et al.,[2]).

Propulsion arises from hydrodynamic reaction forces, which swimmers manipulate by moving their limbs through the water in carefully optimized patterns [39]. Notably, the underwater motion of the hand was traditionally thought to follow a straight path (the so-called "I" pull), but research by Counsilman (1968) showed that elite swimmers often employ an "S"-shaped path composed of lateral sweeps, generating lift forces as a major contributor to propulsion [39]. The "I"-shaped pull yields high forces and is suited for sprint events, while the "S"-shaped pull, though producing lower peak forces, is more energy-efficient and thus preferred for longer distances.

The contribution of other body parts, such as legs and trunk, serves to stabilize the body and support optimal limb movement. For example, flutter kicks help maintain hip stability [39]. However, the primary propulsive elements remain the upper limbs. The movement of the wrist, elbow, and shoulder joints during different stroke phases varies significantly in both magnitude and timing. Peak torques occur during the pull and push phases, with minimal torque during the recovery and entry phases [40]. These torque peaks are substantial for each joint and are greater for the more proximal joints: wrist torques peak at approximately 17 Nm, elbow torques at 85 Nm, and shoulder torques at 176 Nm [40].

A widely used segmentation distinguishes the following main phases: *entry-and-catch* (hand enters and engages with the water), *pull* (hand moves backward under the body), *push* (final underwater propulsion), and *recovery* (arm motion over the water before the next entry) [41]. Each phase is characterized by specific kinematic patterns and force outputs. For example, the beginning of the pull phase corresponds to a distinct increase in mediolateral angular velocity of the lower arm, while the start of the push phase is marked by a reversal in angular motion [42]. The end of the underwater stroke and the start of recovery can be detected via angular transitions in the shoulder and elbow as well as decreasing angular velocity values.

Detecting these phases in real-time is a non-trivial task. Traditional underwater video analysis faces limitations due to refraction at the air–water interface [39, 43], making it difficult to apply optical motion capture. Therefore, IMU-based analysis has gained popularity as a practical alternative. By measuring angular velocity and acceleration, IMUs can provide continuous data during swimming, even in the presence of occlusion or complex limb motion.

Regaieg et al. proposed an automated algorithm for stroke phase detection using an IMU placed on the lower arm [42]. Their method specifically segments the freestyle stroke into the following events:

- **Start of Pull:** Identified by a marked decrease in mediolateral angular velocity (gyro Y, see Figure 2.3), often combined with an acceleration shift along the anterior–posterior axis. This event typically corresponds to the initiation of the downward and backward movement of the forearm, and trigger values are observed when the forearm's y-axis velocity drops below approximately -50cm/s.
- **Start of Push:** Detected as the next significant local maximum in the gyroscope signal along the medial-lateral axis (gyro Y), following the pull onset. This reflects the transition from the insweep to the upsweep phase as the arm begins propulsive extension.
- **Recovery Onset:** Defined by a consistent decline in the magnitude of angular features, such as wrist or forearm angular velocity, and often associated with a reduction in the forearm-to-sacrum angle on the anterior–posterior axis. This signals the transition from underwater propulsion to the over-water return phase.



Figure 2.3: Orientation of the IMU axes used in this study. The orange box indicates the IMU placement.

This threshold-based segmentation approach enables real-time phase recognition suitable for closed-loop control of swimming prostheses. With appropriate adaptations, it could also be extended to para-swimmers, whose stroke mechanics may differ from those of able-bodied individuals due to limb absence or asymmetry. By relying primarily on gyroscope and accelerometer features rather than complex optical tracking, the algorithm remains robust even under water surface occlusion and provides a practical framework for real-time prosthetic control in aquatic environments.

Importantly, the duration and shape of each phase can vary between swimmers and are often adjusted dynamically to optimize performance [44]. The catch phase, for example, is typically very short and often blends directly into the pull phase. Moreover, muscular effort and hydrodynamic loading are difficult to quantify directly, which adds another layer of complexity to understanding propulsion [45].

In this work, we focus on utilizing forearm angular velocity obtained from an IMU as a basis for detecting the main phases of the front crawl stroke. While this method has its limitations — including potential noise and lack of direct force feedback — it remains one of the most accessible and practical solutions for real-time, wearable phase recognition in aquatic environments.

2.5 Swimming with Limb Absence

Despite the presence of physical impairments, individuals with upper limb absence are capable of swimming effectively and often without prosthetic assistance [15]. However, while this approach can enable locomotion, it often introduces biomechanical asymmetries that may lead to long-term musculoskeletal strain or injury. These asymmetries arise from an imbalance in propulsive force generation between the intact and deficient limbs, and from compensatory movement patterns that disrupt stroke symmetry. As such, prosthetic intervention—particularly in the context of training—may not only facilitate propulsion but also promote muscular symmetry and reduce injury risk by balancing load distribution across both sides of the body [15].

Although swimmers with limb absence can generate meaningful propulsion using the residual limb during specific phases—such as the push phase of the stroke—they are generally less effective during phases like the end of the pull, which rely heavily on the presence of a hand and forearm [15]. Quantitative assessments have confirmed that swimmers with upper limb absence demonstrate reduced propulsive force output during tethered sprint trials, despite maintaining similar stroke rates to able-bodied swimmers during the initial

effort [15]. However, as fatigue progresses, swimmers with limb absence experience a more rapid degradation in stroke rate, often accompanied by increased intracyclic fluctuations in swimming speed—up to 35%—due to propulsion imbalance.

Performance gaps are also evident at the competitive level. For example, the world record times (as of 2012) for swimmers with unilateral arm absence over 100 m are 15–20% slower than those of able-bodied athletes [15]. This is attributed not only to reduced propulsive surface area but also to compensatory strategies such as pausing one limb's movement to synchronize with the unaffected side, or reducing pull duration on the impaired side by as much as 40% [42]. Moreover, asymmetries in upper limb kinematics and coordination (e.g., inter-limb coordination index, IdC) persist regardless of breathing technique, highlighting fundamental biomechanical divergence between para and able-bodied swimmers [42].

Interestingly, some evidence suggests that para swimmers adapt their movement patterns to optimize performance despite their impairments. Satkunskiene et al. reported that para swimmers may extend the pull phase to 28% ($\pm$6.2%) of the total stroke duration to compensate for unilateral limitations [42]. Additionally, the residual limb often completes the underwater stroke phase faster than the intact arm due to its reduced mass and length, leading to further asymmetry in joint loading and timing [14].

Efforts to address these imbalances via prosthetics have shown mixed results. For example, Nakashima et al. [14] explored the use of a custom swimming paddle for a swimmer with a unilateral transradial deficiency. While the paddle improved swimming speed overall, it was found to be too large relative to the swimmer's capacity on the impaired side, potentially due to muscular weakness around the residual limb. This led the authors to question the assumption that joint effort should be equalized between impaired and unimpaired limbs; rather, prosthetic design must consider asymmetrical strength and stroke dynamics.

The underlying gap lies in the limited integration of real-time sensing and adaptive control in swimming prostheses. Most current research focuses on general kinematic assessment, not dynamic compensation or augmentation via wearable robotics. The need for intelligent systems that can detect stroke phase transitions and modulate assistance accordingly remains unmet—particularly for para swimmers with asymmetrical stroke profiles. Given the demonstrated feasibility of IMU-based stroke segmentation [42], this represents a promising direction for enhancing swimming performance and safety through prosthetic intervention.

Chapter 3

Kinematics Analysis

Understanding the biomechanics of swimming is essential for the development of effective control strategies for adaptive prostheses. To capture the complexity of arm movement in swimming and to inform the design of a phase-based prosthetic wrist controller, two complementary datasets were utilized. Each dataset addresses specific challenges related to aquatic motion analysis and provides unique insights necessary for building a robust control system.

The first dataset consists of real-world recordings collected using a dual-media motion capture system, which synchronizes underwater and overwater cameras to capture natural arm movements during freestyle swimming. This approach offers the advantage of ecological validity by observing swimmers in their natural environment, directly capturing the interaction between the limb and water. However, aquatic motion capture inherently faces challenges such as surface reflections, marker occlusion, and interference from water turbulence and bubbles. These factors contribute to limitations in data quality, notably short recording durations and occasional noise artifacts, restricting the dataset to brief segments of swimming motion. To mitigate these limitations, complementary data were obtained from controlled dry-land simulations using an inertial measurement unit (IMU)-based motion capture system.

3.1 Swimming Kinematics Dataset

The aquatic kinematic data were provided by LABIOMEP and CIFI2D at the University of Porto and include joint angles and angular velocities of the forearm during freestyle swim-

ming for two subjects (one male, one female). The data collection employed a state-of-the-art dual-media motion capture system (Qualisys AB, Sweden), which allows simultaneous tracking above and below the water surface. Calibration was performed involving both individual wand calibrations and a combined underwater–overwater calibration procedure to ensure accurate spatial alignment between the two camera sets. One camera system was designated as the global reference ("master") while the other acted as the synchronized "slave", ensuring temporal alignment of recordings.

Despite these careful calibrations, challenges inherent to aquatic environments affected data quality. Water surface reflections created transient false markers ("ghost markers"), while water turbulence and bubbles caused intermittent marker occlusions. These artifacts were detected and removed by analyzing residual errors and temporal continuity. Trajectory gaps, particularly near the water interface, were interpolated using polynomial methods and rigid body assumptions to reconstruct plausible joint trajectories. In rare cases involving multiple missing markers, a predefined biomechanical skeleton model was used to fill data gaps. Smoothing techniques further reduced noise without distorting the underlying movement patterns.

The processed dataset, though carefully refined, remains limited by its short capture window—each recording contains approximately one full stroke cycle of a single arm. Consequently, the data do not provide continuous or repetitive stroke patterns necessary for robust statistical analysis or machine learning. Figure **??** illustrates typical data quality for one trial, showing wrist flexion-extension as the primary movement of interest for this project, alongside elbow angular velocity, which—according to the literature review—is a key signal used to identify the phases of the swimming stroke. The recorded motion is not smooth or perfectly repetitive, reflecting both the complexity of aquatic motion capture and the natural variability of swimming strokes.

This dataset's strengths lie in its direct representation of natural swimming biomechanics and the interaction with aquatic forces, which are difficult to replicate in dry-land simulations. However, the brevity and noisiness of the data limit its applicability for prosthetic control design without additional data collection.

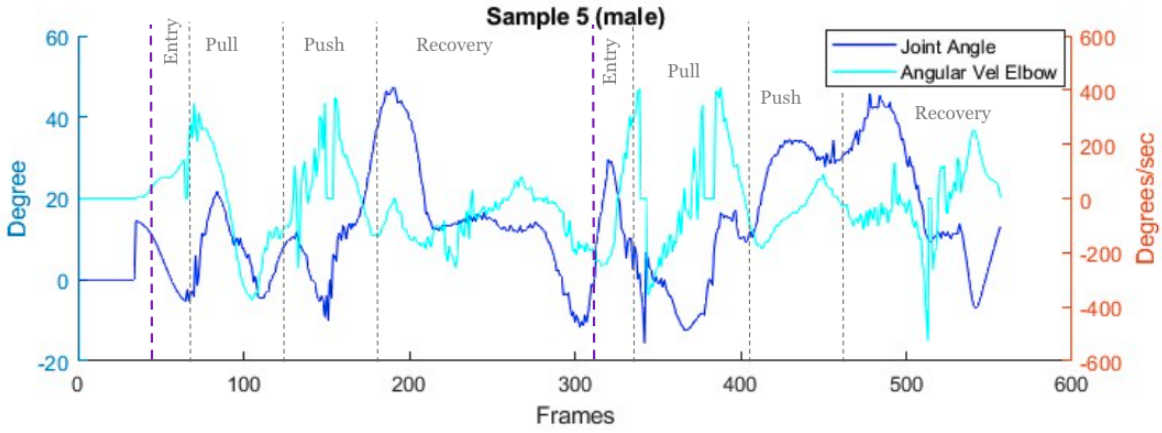


Figure 3.1: Sample kinematic data from one swim trial showing wrist joint angle (sagittal plane) and elbow joint angular velocity.

3.2 Kinematic Data from Dry-Land Swimming Trials

To address the limitations of aquatic motion capture, a second dataset was collected at the University of Waterloo using the Xsens MVN Awinda system (Xsens Technologies B.V., Enschede, The Netherlands), a full-body IMU-based motion capture setup. This system includes 17 inertial measurement units sampling at 100 Hz, enabling detailed tracking of joint angles and angular velocities without occlusion or optical interference. IMUs were placed according to the manufacturer's full-body configuration (see Figure 3.2), providing comprehensive biomechanical data during simulated front crawl swimming motions.

Data were collected from a single healthy female participant (22 years old, 169 cm, 59 kg) with amateur swimming experience. The participant performed front crawl arm movements while lying prone on a bench, simulating swimming strokes in a controlled dry-land environment. This setup (see Figure 3.3) allowed uninterrupted data capture over extended periods, free from the challenges of underwater tracking, and enabled collection of multiple stroke cycles (at least 10 per trial).

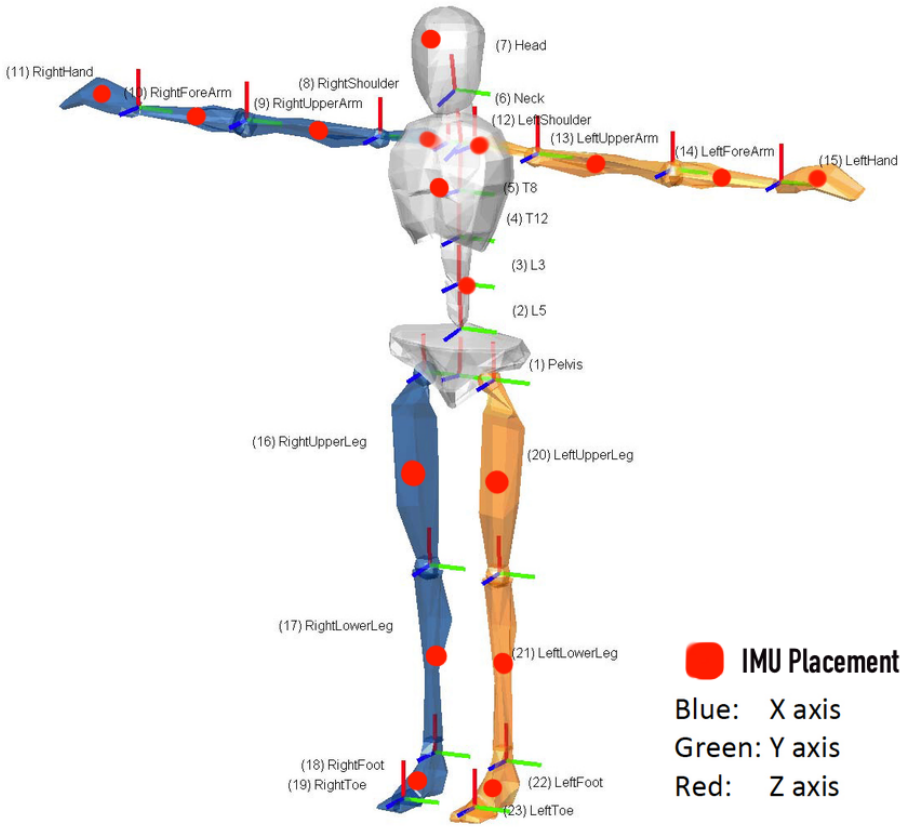


Figure 3.2: Placement of Xsens MVN Awinda IMUs used for full-body motion capture and axis of segments (Modified from [3]).



Figure 3.3: Experimental setup for dry-land swimming simulation using the Xsens MVN Awinda motion capture system with global axes at the University of Waterloo.

Though this method lacks direct interaction with the water's hydrodynamics, it offers high-fidelity, noise-free data and repeatable motion cycles critical for developing and validating prosthetic control algorithms. Additionally, full-body capture facilitates future studies on intersegmental coordination, such as trunk rotation and contralateral limb movement, which may influence prosthetic control strategies. Nevertheless, it should be acknowledged that the dry-land setup inherently alters the swimming motion: the absence of water resistance may lead to faster execution, shorter durations of specific stroke phases, and increased difficulty in coordinating movements without continuous hydrodynamic feedback.

Only data from the right arm were analyzed for the prosthesis control design. Representative kinematic data, including wrist flexion-extension angles and forearm angular velocity, demonstrate clear periodicity and consistent stroke phases suitable for phase segmentation and real-time control (see Figure 3.4).

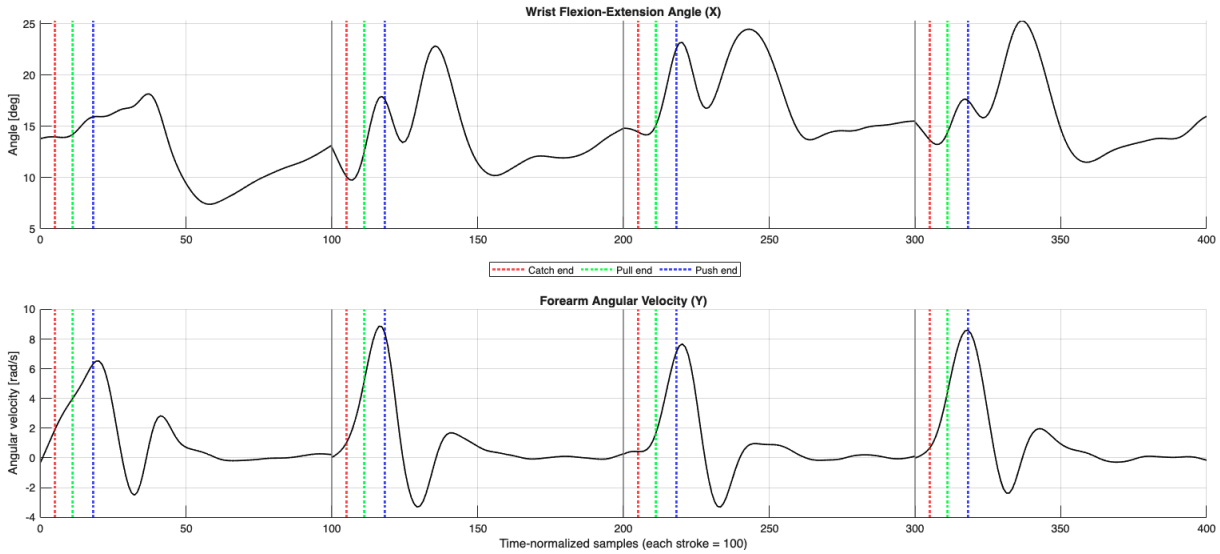


Figure 3.4: Flexion/extension of the wrist (top plot) and corresponding forearm mediolateral angular velocity measured by an IMU (bottom plot) over four consecutive strokes. Vertical dashed lines denote stroke phase transitions: red for the end of the catch, green for the end of the pull, and blue for the end of the push.

Comparing Figure 3.4 with Figure 3.1, the overall patterns appear broadly similar, although some differences are evident. These discrepancies may result from the relatively short duration of the aquatic dataset and potentially higher signal noise due to environmental constraints during recording. Additional variations in the kinematic profiles could arise from differences in the anthropometric characteristics of the subjects (one male, one female), from unknown swimming skill levels of the participant in the aquatic data collection, and from variations in swimming technique, since certain techniques can lead to markedly different forearm rotation patterns during the recovery phase.

3.3 Data Processing and Stroke Phase Segmentation

Raw data from both datasets underwent preprocessing, including filtering and smoothing to reduce noise and eliminate artifacts. A zero-lag fourth-order Butterworth low-pass filter with a 6 Hz cutoff frequency was applied, balancing noise reduction and signal fidelity.

Stroke cycles were manually segmented through visual inspection of joint angle trajectories, identifying key events corresponding to different stroke phases. An average stroke

cycle was computed from multiple repetitions, providing a representative kinematic profile for control algorithm development.

Figure 3.5 shows the mean wrist flexion–extension profile together with forearm angular velocities around the Y- and Z-axes relative to the pelvis, derived from dry-land IMU recordings across five trials and multiple stroke cycles, with phase segmentation. Shaded bands represent ± 1 standard deviation. capturing natural motor variability typically observed in both healthy swimmers and potential prosthesis users with impaired motor control. The signals are segmented into distinct kinematic phases.

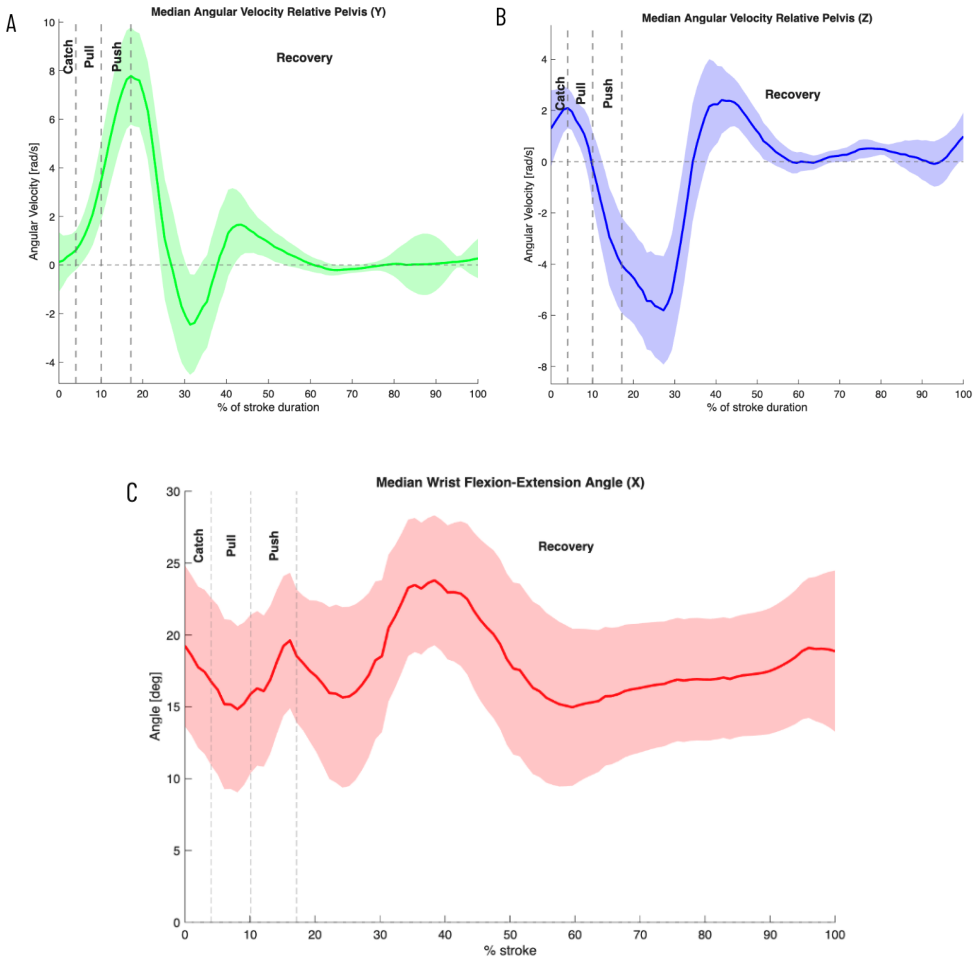


Figure 3.5: Mean kinematic profiles of the right-hand wrist during a representative front crawl stroke. (A) Angular velocity of the forearm around the Y-axis relative to the pelvis, with phase segmentation. (B) Angular velocity of the forearm around the Z-axis relative to the pelvis, with phase segmentation. (C) Wrist flexion-extension angle, with phase segmentation. The shaded areas represent the standard deviation across trials.

The variability that can be observed on the plot might be caused by dry land setup of data collection since there was no resistance during this movements that usually serve as a feedback for swimmers in water. Variability in joint angles and angular velocities underscores the importance of developing control systems robust to natural movement fluctuations. Moreover, it emphasizes the necessity for user-specific calibration to accom-

modate differences in swimming technique, limb anatomy, and rehabilitation stage.

The kinematic data collected from real swimming trials were not directly used for prosthesis control but served to validate and contextualize the dry-land IMU dataset. Aquatic recordings provide insights into natural stroke mechanics, hydrodynamic interactions, and inter-limb coordination, enabling identification of typical ranges for wrist angles, forearm angular velocities, and stroke phase durations. Dry-land trials, in contrast, offered controlled, repeatable measurements across multiple cycles, forming the basis for developing the phase-based wrist controller. By comparing both datasets, it was possible to ensure that the dry-land motions adequately reflected realistic swimming patterns, while also highlighting variability and potential deviations caused by the absence of water resistance. These analyses inform quantitative design criteria—including angular ranges and phase thresholds—supporting the creation of a biomechanically grounded and user-adaptable prosthetic control strategy.

Chapter 4

Design

To address the limited availability of swimming-specific prosthetic devices for individuals with upper limb amputation, we propose the development of an active prosthesis with one degree of freedom. Existing commercial solutions are scarce, often focusing on general daily activities rather than sport-specific applications, and those that do exist for swimming are typically passive, offering no adaptability to the user's stroke. Our design aims to bridge this gap by introducing a mechanism that actively responds to the motion phases of the freestyle stroke, thereby enhancing performance and comfort in the water. This chapter outlines the step-by-step design process of the device, from initial concept to final prototype.

4.1 System Requirements

The development of a functional prosthetic device for swimming must be guided by both general user expectations and the specific demands of the aquatic environment. Survey data on upper limb prosthesis users indicate that the most common reasons for dissatisfaction are related to comfort (61%), weight (52%), and insufficient functionality (43%). Aesthetic appearance was mentioned as a concern by only 26% of respondents. Among individuals who chose to abandon prosthesis use altogether, 70% cited lack of comfort and excessive weight as primary reasons, followed by poor functional performance (50%) [46].

In the context of swimming, additional domain-specific requirements emerge. The system must respond quickly and accurately to the phase of the stroke, necessitating low-latency sensing and actuation. Moreover, all components must be enclosed in a waterproof

housing to prevent failure or corrosion. The final device must also be compact and unobtrusive to avoid impeding arm movement or generating drag.

Based on this, the priority design requirements for the device include:

- **Comfort** — the center of mass and weight distribution should promote a comfortable feel; to achieve this, the heaviest components of the prototype should be positioned closer to the proximal end;
- **Weight** — should be close to or lower than that of the amputated hand to reduce fatigue and preserve natural swimming biomechanics;
- **Functionality** — the prosthesis should dynamically assist or replicate wrist motion in response to the stroke phase;
- **Water resistance** — as the device will be fully submerged and exposed to dynamic water pressure;
- **Energy efficiency and portability** — it should operate autonomously for the duration of typical training sessions without external power sources;
- **Aesthetics** — secondary, but still relevant for long-term user acceptance.

Meeting these requirements will ensure that the device not only performs its intended function but also promotes consistent and comfortable use, both during training and rehabilitation sessions.

In terms of user interaction, the prototype has only basic controls. The motor can be quickly disconnected using a dedicated switch, while the control board is powered simply by connecting the battery wires to the socket. Two LEDs provide feedback: one indicates whether the motor is active, and the other shows the battery status of the electronics. The prosthesis begins operation automatically once swimming motion is detected, without further user input.

The device is intended for use in both pools and open water. Although designed with training and rehabilitation scenarios in mind, it is not suitable for competitive environments. The attachment system for securing the prosthesis to the residual limb was not a focus of this work.

4.2 Mechanical Design

The developed prototype is a swimming-specific prosthetic arm aimed at supporting both rehabilitation and performance improvement for individuals with transradial limb loss. The design features a rigid forearm structure that houses the main components, including the electronics, inertial measurement unit (IMU), batteries, and motor. The motor is connected through a transmission system to the wrist joint, where it drives a shaft securely fixed to the hand section. The hand itself is designed with a fixed palm to provide consistent interaction with the water, while the actuated wrist enables controlled rotation synchronized with the swimming stroke phases (see Figure 4.1).

Embedded electronics, consisting of the IMU and microcontroller, continuously detect stroke dynamics and adjust the wrist angle in real time. This approach allows for smoother and more natural movement patterns in the water, reducing compensatory strain and encouraging balanced muscle engagement. The overall system is optimized for compactness, energy efficiency, and reliability under repetitive aquatic loading, with the modular architecture enabling further refinement and adaptation to different swimming techniques.

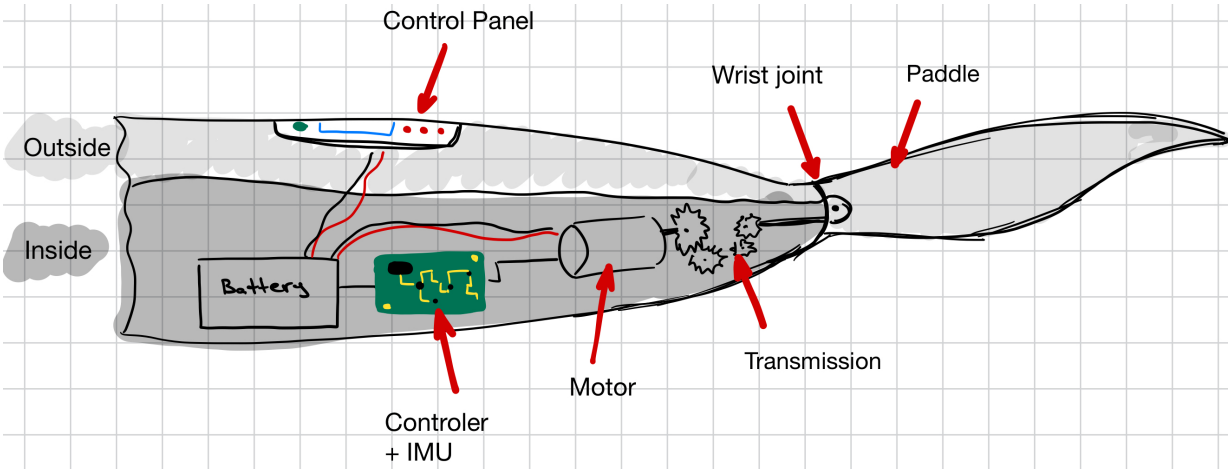


Figure 4.1: Concept art of the proposed prototype.

4.2.1 CAD Models

The complexity of the human body shape necessitates flexible modeling approaches that are often difficult to implement using traditional Computer-Aided Design (CAD) tools alone, due to their inherently parametric and constraint-based structure [47, 48, 49]. In

contrast, polygonal modeling—also referred to as digital sculpting—enables the creation of anatomically realistic and organically shaped structures, although it generally lacks the dimensional precision and tolerance control required for engineering applications [50, 51, 52]. Therefore, a hybrid approach was adopted in this project: polygonal modeling was used to capture the anatomical geometry of the hand, while CAD modeling supported mechanical integration and engineering constraints.

To obtain a realistic human hand shape, an open-source poligonal 3D model—commonly used in game development and animation pipelines—was utilized [53]. Although primarily designed for animation, the model was developed using polygonal techniques, making it suitable for anatomical replication. The rigged model was imported into Blender (Blender Foundation, Amsterdam, The Netherlands), an open-source 3D modeling and animation software, where it was posed into the desired configuration. Thin connecting surfaces between the fingers (representing inter-digital webs) were then added, the mesh was trimmed to the required length, and the geometry was prepared for export.

The processed model was subsequently imported into Fusion 360 (Autodesk Inc., San Rafael, CA, USA), where it was scaled to match anatomical dimensions (mean upper arm length and mid-upper arm circumference for adult males [54, 55]) and converted into a solid body suitable for mechanical design and fabrication. The resulting geometry was segmented into smaller components, each tailored to accommodate the intended mechanisms, and optimized for 3D printing and assembly. The design of each subcomponent is detailed in the following sections.

Throughout the modeling process, design choices were guided by additive manufacturing constraints, including minimum wall thicknesses, dimensional tolerances, and the need for reliable inter-part connections. These constraints ensured that all components were manufacturable and mechanically robust.

4.2.2 Hand Shape

One of the key design requirements was to replicate the natural shape of a human hand. This choice aimed to improve the aesthetic acceptance of the prosthesis, reducing rejection rates associated with appearance-related discomfort. Beyond visual realism, mimicking the human hand shape supports biomechanical symmetry, such as by matching weight and center of gravity, ensuring balanced muscular loading and natural force distribution during movement.

Since the hand is the primary surface responsible for generating propulsion in front crawl swimming [15], its shape significantly affects performance. A literature review iden-

tified optimal finger and thumb positions to maximize drag and thus swimming efficiency. According to van den Berg et al. [56], cupping the hand reduces drag by nearly 6%, making it less effective for propulsion. Their study showed that a flat hand with a 5° finger spread and abducted thumb provides the highest drag, while thumb flexion only minimally influences hydrodynamic resistance.

However, in the context of upper-limb absence and possible muscle weakness on the residual side, replicating the exact optimal shape may not be practical or sustainable for long-term use. Therefore, the chosen design compromises between optimal hydrodynamic performance and functional simplicity. The fingers were positioned close together, with the thumb in slight flexion to preserve general hand geometry. Additionally, to facilitate 3D printing and enhance structural robustness, the fingers were connected with a thin unifying structure that visually resembles a swimming glove.

The design was optimized for fused deposition modeling (FDM) 3D printing on a Bambu Lab P1S printer, with a build volume of 256 × 256 × 256 mm, taking into account the printer's size limitations and minimizing the need for support structures during fabrication. This ensured better print reliability and post-processing efficiency.

To support future customization and testing of different hydrodynamic profiles, the palm and fingers were designed as a detachable module that can be easily replaced with alternative printed versions. This modularity enables rapid prototyping of different hand geometries or personalization to individual users' anatomical characteristics or performance needs.

The final CAD model of the prosthetic hand is shown in Figure 4.2.

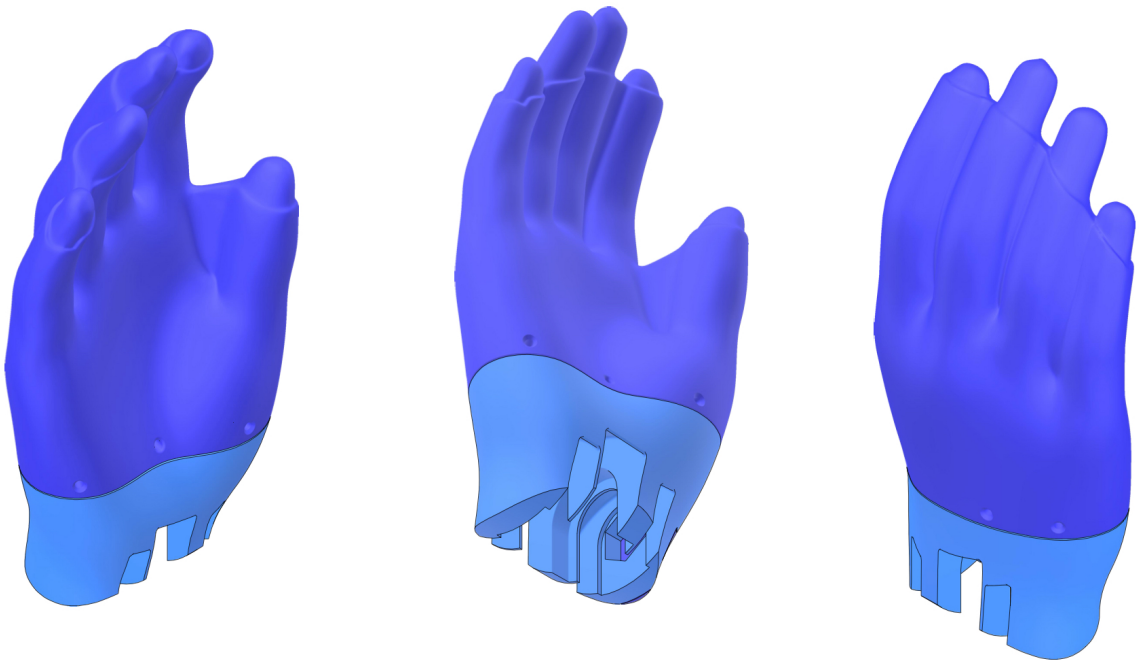


Figure 4.2: CAD rendering of the prosthetic hand design (three perspectives).

4.2.3 Wrist Joint Mechanism

To ensure a more natural feeling of the prosthesis, the center of mass of the prototype should be located closer to the proximal end, near the future socket attachment [25]. This requires placing the heaviest components, such as the servo motor, as close as possible to the socket. However, the actual axis of the wrist joint does not coincide with the most proximal position available for the motor. To overcome this constraint, a transmission mechanism is needed to connect the servo motor to the wrist shaft while allowing the motor to be positioned further proximally.

For this purpose, a belt drive mechanism was selected. Although not necessarily the optimal long-term solution, it serves as a functional starting point that can be upgraded in future iterations. The belt drive consists of two pulleys connected by a timing belt. In this design, the pulleys have a tooth ratio of 20:60, which increases the torque at the output shaft by a factor of approximately three. This amplification allows the wrist joint to handle greater resistance despite the limited torque generated by the servo.

While relatively simple to implement, the belt drive introduces certain design con-

straints. One of them is the need for a tensioning system to maintain consistent belt engagement, which is discussed further in the forearm design section.

A critical component of the wrist mechanism is the rotational shaft that connects the output pulley to the hand section. This shaft must withstand mechanical loads during motion, securely fix the hand component, and maintain reliable engagement with the pulley to ensure effective torque transfer. To implement this in a simple, robust, and accessible manner, an M10 hex bolt was repurposed as the shaft.

Using a standard bolt avoids the need for custom-machined shafts, which could provide more precise tolerances but would increase manufacturing complexity and cost. The M10 bolt, by contrast, fulfills all functional requirements: it prevents pulley slippage in the 3D model, provides sufficient mechanical strength for expected loads, and remains easy to source and replace.

Only a portion of the bolt was threaded, with the remaining section left smooth to ensure structural integrity and provide adequate friction for mounting rotating components. This design effectively replicates the function of a shoulder bolt, although it was implemented using a modified standard bolt. To prevent the pulley from slipping on the shaft, a shallow recess was drilled into the bolt surface to accommodate the tip of a set screw, creating a secure mechanical stop without introducing weak points as a fully drilled hole would. This reinforcement is particularly important given the high rotational forces expected during operation; without it, the pulley could rotate independently of the shaft, compromising torque transmission and propulsion efficiency.

The shaft implementation is illustrated in Figure 4.3, showing how the M10 hex bolt serves as a functional, reliable rotational axis.



Figure 4.3: M10 hex bolt repurposed as a wrist shaft.

The CAD model of the wrist joint (Figure 4.4) was designed to house the output pulley, shaft, and associated mechanical components, and to serve as an interface between the forearm and hand sections of the prototype. The geometry supports a functional range of motion of approximately $\pm 30^{\circ}$, as required by the application. Internal cavities and mounting features were tailored to maintain compactness while ensuring the precise fit of each component.

To fix the main shaft securely in place, a hexagonal recess was modeled to accommodate the bolt head, preventing rotation. A removable clamping cap—tightened with a bolt—was added to apply axial constraint and ensure the bolt remains stationary. For future disassembly, a small access hole was drilled from the opposite side of the wrist after full assembly.

To reduce friction and enhance mechanical performance, washers were inserted between plastic components. This also contributes to long-term durability under load.

Fit tolerances were carefully designed to account for typical inaccuracies in 3D printing and component geometry. These values were validated using test prints, ensuring that unwanted plastic-on-plastic contact was avoided while maintaining secure and aligned assemblies.

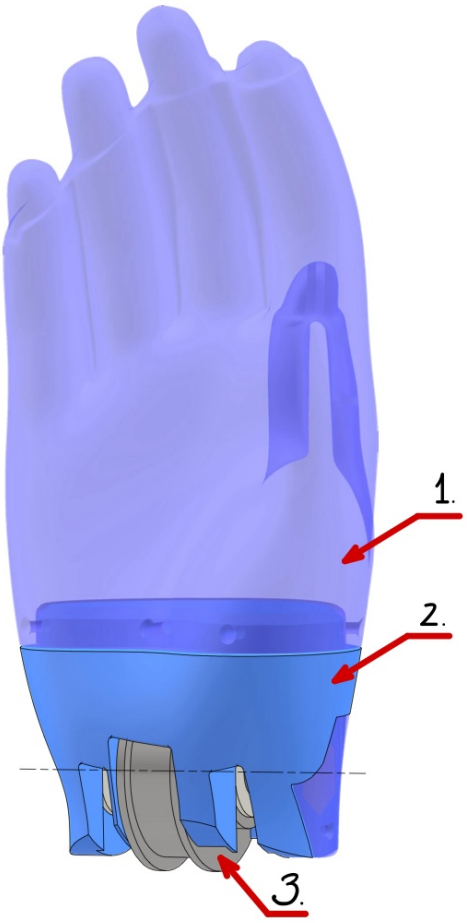


Figure 4.4: Wrist joint CAD model. The dashed line indicates the wrist joint axis. (1) Hand part, (2) Wrist part, (3) Pulley.

4.2.4 Forearm

The forearm component serves as the primary housing for all internal components of the prosthesis, including batteries, the servo motor, and control electronics. While accom-

modating these components, the external shape was designed to approximate the natural contour of a human forearm for aesthetic consistency. However, because the prototype's proportions were initially based on the hand size, increasing the internal volume of the forearm would have required an unrealistic enlargement of the hand. To address this limitation, two external enclosures were added: one to house the servo motor and another to mount the control board (see Figure 4.5). These extensions allowed the design to remain compact while providing sufficient space for hardware.

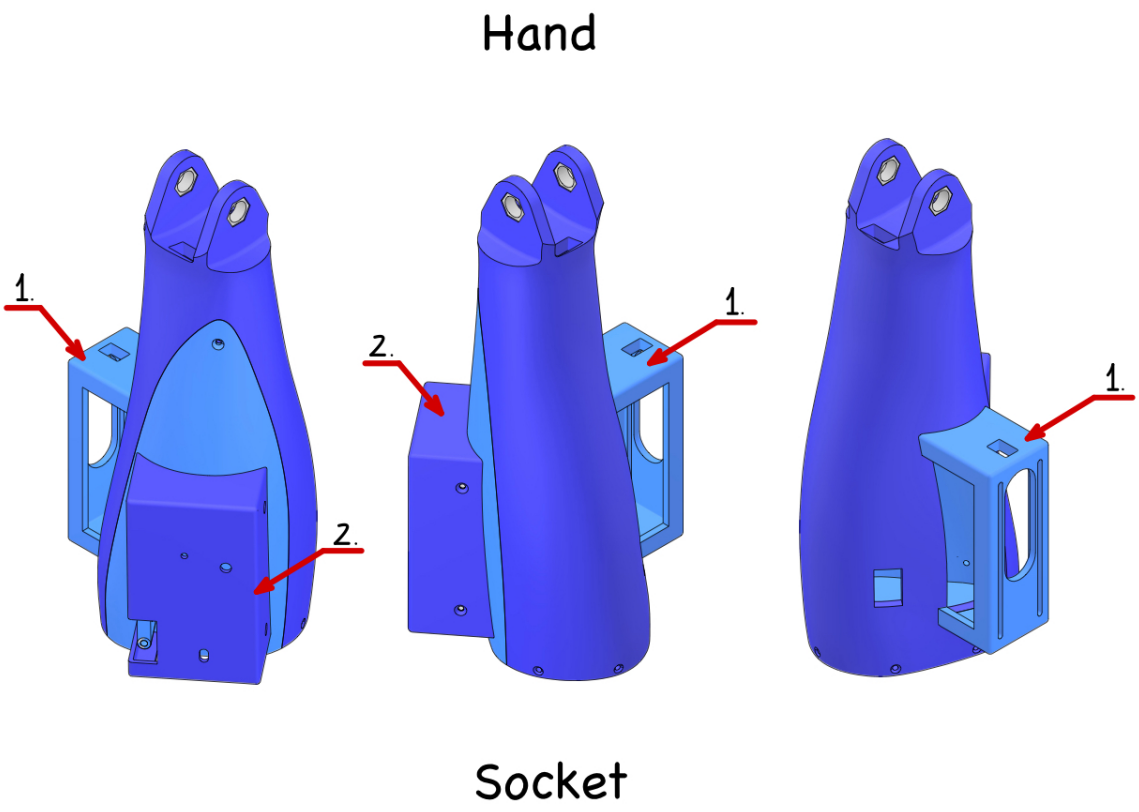


Figure 4.5: Forearm CAD model showing external compartments in three views. Key components are indicated as follows: (1) enclosure for the servo motor, (2) enclosure for electronics.

The servo motor enclosure features a set of custom-designed mounting brackets that

fulfill both alignment and belt tensioning functions (see Figure 4.6). The motor is seated within slotted mounting rails *(3)*, allowing it to slide longitudinally prior to final fixation. Six screws, each coupled with washers *(1)*, are inserted through elongated holes and tightened to lock the motor in its desired position. This configuration enables precise adjustment of belt tension while maintaining alignment between the pulleys, effectively reducing slippage and ensuring consistent torque transmission.

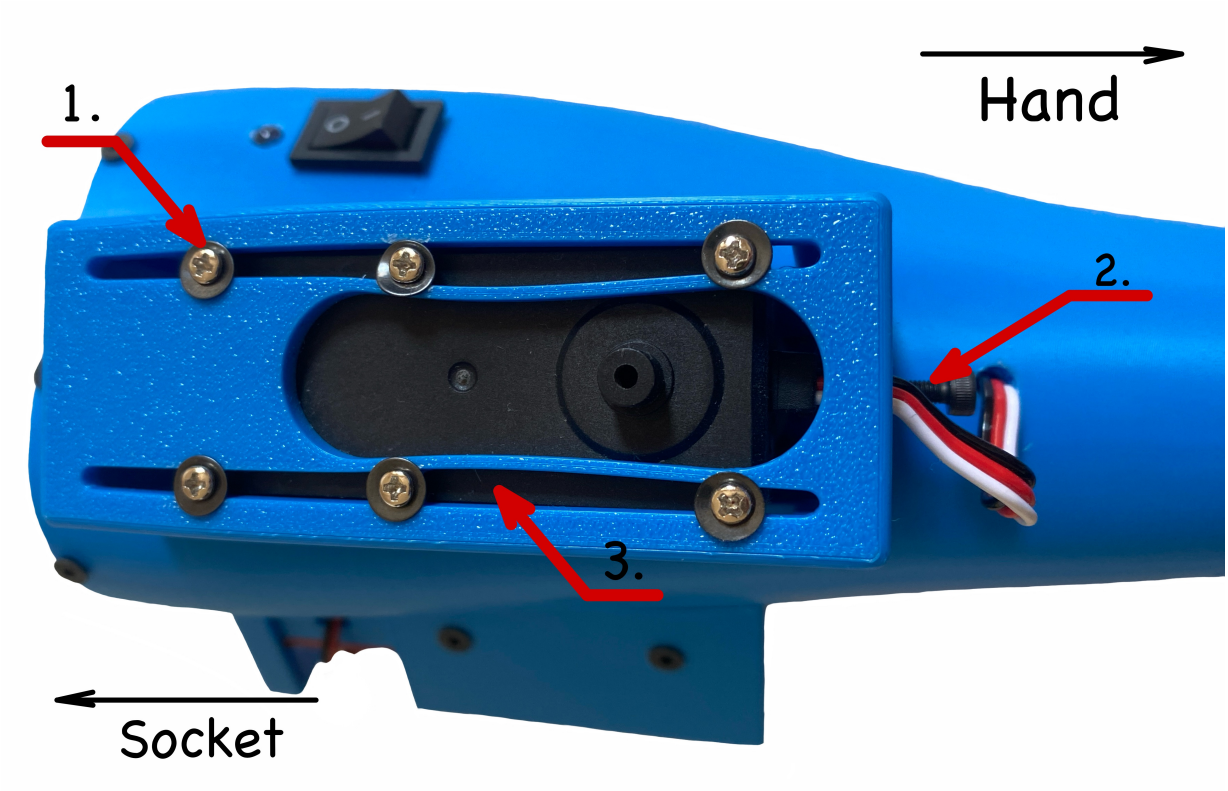


Figure 4.6: Servo motor enclosure with custom tensioning mechanism. Key components: (1) screws with washers that clamp the motor position, (2) vertical screw providing additional stabilization, (3) slotted mounting rails that allow the motor to slide during adjustment.

To further stabilize the motor and prevent wobble or long-term loosening under dynamic load, an additional screw is inserted from the vertical direction (2) (Figure 4.6). This screw applies a downward preload, pressing the motor securely into its mount and reducing any residual play that might occur despite horizontal clamping.

To optimize material usage and reduce print time for this component, the lateral walls of the mounting brackets were deliberately removed. This design choice preserved structural integrity while significantly streamlining the 3D printing process.

To facilitate fabrication and assembly, the forearm structure was divided into three separate parts (see Figure 4.7):

- The **main housing**, which holds the motor, batteries, and most wiring;
- The **side lid**, which provides full access for maintenance and secures the control board;
- The **button lid**, which primarily facilitates 3D printing by closing the bottom opening and assisting in minor mounting tasks, while not being used for routine maintenance access.

All parts were designed with a uniform wall thickness of 5 mm to ensure sufficient structural strength while maintaining reasonable print time and material usage. The overall structure of the forearm component is illustrated in Figure 4.5.

The control board is held by two lateral support brackets that ensure stable positioning. A protective top lid covers the assembly, safeguarding the electronics against mechanical impact or damage.

The top of the forearm terminates in two U-shaped structural extensions that interface with the wrist assembly. These extensions serve as mounting brackets for the rotating shaft that connects the wrist mechanism and hand to the forearm structure. To accommodate the transmission belt, dedicated cutouts were added at the distal end of the forearm, allowing the belt to pass through without interference. Internally, the forearm includes hollow cavities to house components, which may create enclosed air pockets. These pockets could affect the buoyancy of the prototype in water and should be considered in future waterproofing or hydrodynamic adjustments.

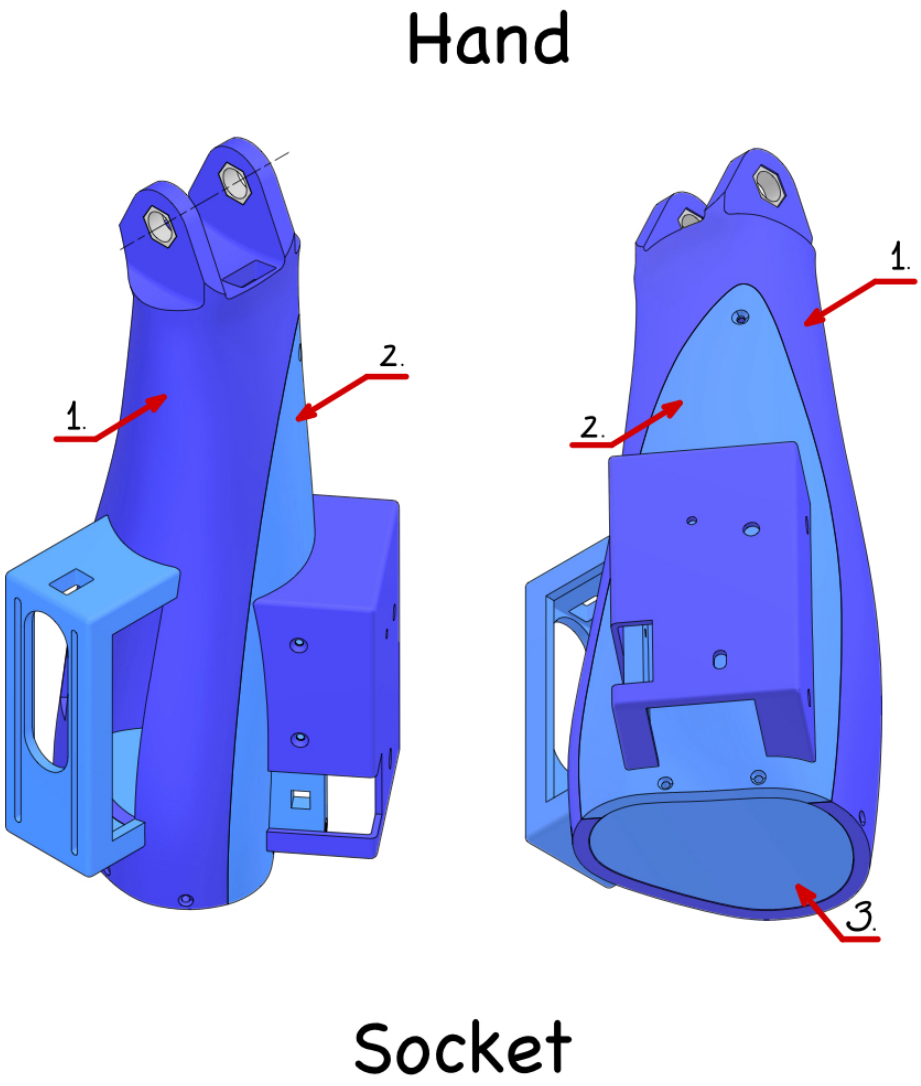


Figure 4.7: Forearm CAD model in two views. Key components are indicated as follows: (1) main housing, (2) side lid, (3) button lid.The dashed line represents the wrist joint axis.

4.3 Control System Design

The core concept behind the control system is to develop a biomechanically informed approach that replicates the natural wrist motion observed during front crawl swimming. The system relies on real-time input from an inertial measurement unit (IMU) mounted on the forearm of the device. In our implementation, both the mediolateral (ω_Y) and vertical (ω_Z) components of the forearm angular velocity were used to determine the swimmer's current stroke phase. This approach extends previous methods that primarily relied on the mediolateral component [42, 41], and was motivated by the observation that combining ω_Z and ω_Y provides more robust identification of the transitions between the catch, pull, push, and recovery phases of the freestyle stroke.

As outlined in the literature, the swimming cycle can be divided into four main phases: entry-and-catch, pull, push, and recovery. The pull and push phases may also be further subdivided into downsweep and insweep, and upsweep and exit, respectively. This finer subdivision of the pull and push phases reflects distinct biomechanical events within each stroke, such as changes in hand trajectory or orientation, which have been shown to influence propulsion efficiency and muscle activation patterns [44]. Each of these phases is characterized by distinct motion patterns, which can be detected through IMU signals, as demonstrated in prior work [42]. The control strategy implemented in this prototype is based on those findings and enables phase-dependent adjustment of wrist angle during the stroke.

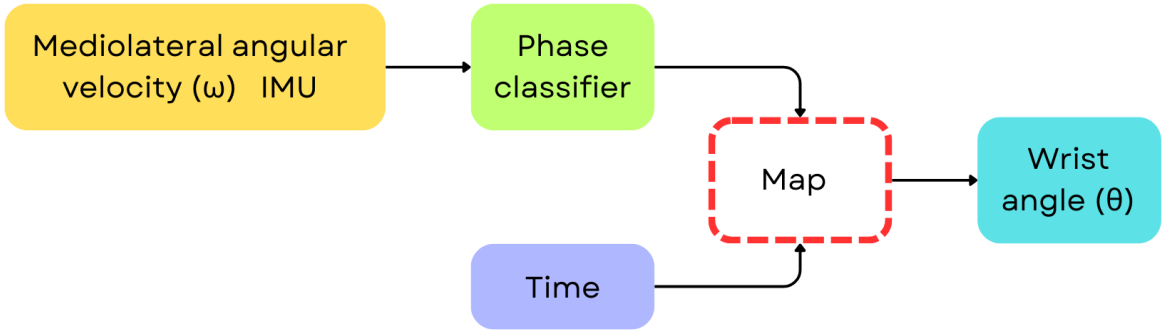


Figure 4.8: Block diagram of phase-based wrist control.

4.3.1 Swimming Phase Detection

To identify the main phases of the swimming stroke, angular velocity is measured from the forearm using an IMU (Adafruit BNO055, $\pm 2000°/s$ gyroscope range, 16-bit resolution). The sensor provides practical measurements with a typical noise level of around $\pm 1°/s$ and an effective resolution of approximately $0.06°/s$. Overall accuracy is influenced by sensor placement, soft tissue movement, and the dynamic nature of swimming motions. Despite these factors, this approach offers a reliable, real-time estimate of stroke phases, sufficient for prototype control without requiring high-end motion capture systems.

This approach draws on prior work such as Regaieg et al. [42], who proposed detailed segmentation strategies based on a broad combination of gyroscopic and acceleration features. In our study, these concepts were adapted to a real-time control setting by focusing on angular velocity signals from the forearm. Phase transitions were identified using threshold-based events in both the mediolateral (ω_Y) and vertical (ω_Z) components. This adaptation allowed us to retain robust phase discrimination while ensuring computational efficiency suitable for real-time prosthesis control.

Due to its inherently short duration, the *entry* phase often transitions almost immediately into the *catch* phase. For this reason, we currently do not distinguish the entry phase explicitly. In future work, this could be improved by incorporating force sensors capable of detecting the moment of hand contact with the water surface, which would mark the onset of the entry phase more reliably.

The automated detection of stroke phases was based on the mediolateral (ω_Y) and vertical (ω_Z) angular velocities of the forearm. A complete stroke cycle was defined as the interval between two successive catch initiations, i.e., from the onset of one catch to the onset of the next. For visualization and analysis, this interval was normalized to cover 0–100% of the cycle time.

The *catch* phase was defined to begin at the onset of the cycle (0%) and to end at the first positive peak detected in ω_Z. The *pull* phase then extended from the end of catch until the first zero-crossing of ω_Z from positive to negative values. Following this, the *push* phase began immediately after pull and lasted until the first positive peak in ω_Y observed thereafter. Finally, the *recovery* phase started after the push phase and continued until the subsequent onset of catch, thereby completing the cycle.

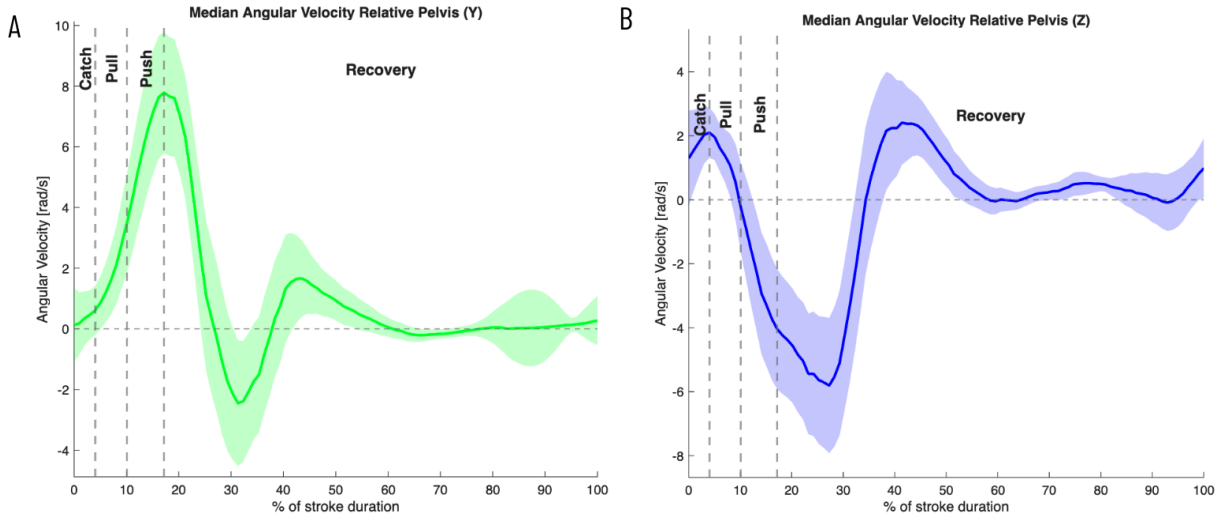


Figure 4.9: Phase segmentation based on the proposed control algorithm using forearm angular velocity (ω_Y and ω_Z). (A) Angular velocity around the Y-axis relative to the pelvis. (B) Angular velocity around the Z-axis relative to the pelvis.

For this control design, angular velocity is selected as the primary input instead of orientation angles. This is motivated by the fact that IMU-based orientation tracking is susceptible to drift over time, whereas angular velocity remains more reliable and relevant to real-time prosthesis control.

4.3.2 Kinematic Mapping

Although the complete front crawl stroke exhibits non-linear and variable dynamics due to changes in speed, posture, and limb coordination, it can be effectively segmented into distinct kinematic phases. Each phase corresponds to a biomechanically consistent movement pattern and can therefore be approximated with a separate mapping from $\vec{\omega}_{\text{forearm}}$ to θ_{wrist}.

To construct these functions, we performed a detailed kinematic analysis of arm motion captured during swimming imitation trials on a gym bench. The analysis was based on motion capture data and focused on wrist orientation and angular velocity, particularly around the mediolateral axis of the forearm. The recorded data were segmented into the canonical phases of the swimming stroke (entry, catch, pull, push, and recovery), based on

threshold criteria applied to the IMU angular velocity data. Each phase was then modeled independently.

For each stroke phase, we extracted the temporal evolution of wrist angle and developed a mapping between $\vec{\omega}_{\text{forearm}}$ and the desired wrist angle. These mappings were implemented as piecewise-linear functions consisting of 2–3 linear segments per phase, chosen to capture the main curvature of the average wrist trajectory. Breakpoints were placed at characteristic changes in slope, identified from the mean kinematic profiles. This decomposition strategy allowed us to reduce system complexity while ensuring sufficient fidelity to the observed motion.

The final mapping functions define the target wrist rotation angle as a function of current stroke phase, which is identified in real-time from gyroscopic cues. Because the prototype employs a belt-driven pulley mechanism to actuate wrist motion, the motor output must be scaled by the effective gear ratio of the transmission system. This mechanical transformation was explicitly included in the mapping, ensuring that the servo commands result in the intended physical wrist rotation.

4.3.3 Implementation Details

The control algorithm was deployed on an Adafruit ESP32-S3 Reverse TFT Feather microcontroller, selected for its built-in display interface and computational performance. The firmware was written in C++ using the Arduino IDE environment. The system integrates an Adafruit BNO055 IMU, interfaced via I^2C, using the corresponding Adafruit library. Real-time PWM-based control of the servo motor is handled by the S3Servo library, which allows flexible signal timing control.

The IMU is sampled at 100 Hz, providing high-resolution angular velocity data. Phase recognition is performed online using a threshold-based logic applied to the angular velocity about the mediolateral axis. Upon detection of a phase transition, the control logic selects the corresponding phase-specific mapping function, which computes the appropriate target wrist angle. This target angle is then converted into a PWM duty cycle and sent to the servo motor. The motor is operated in position (angle) control mode, ensuring that the commanded wrist angle is achieved directly. The entire control loop runs at the same frequency as the IMU sampling, ensuring low-latency response.

The system also incorporates safety constraints and mechanical limits, preventing the motor from exceeding physically feasible rotation angles. These limits were derived from the mechanical design of the wrist joint and the measured maximum range of motion observed during kinematic capture.

4.4 Electrical Design

The electrical system of the device was developed to enable controlled actuation of the wrist joint based on sensor input and predefined motion logic. A key design consideration was ensuring that the actuator could produce sufficient torque to meet or exceed the mechanical demands of active swimming.

As discussed in the literature review, peak wrist torques generated by professional swimmers can reach approximately 17 Nm. Although this prosthesis is not intended for elite athletes, designing for this upper limit provides a valuable safety margin. To satisfy these requirements, a high-torque servo motor (ANNIMOS 150 kg, 12 V) was selected. The motor offers a torque of up to 15 Nm and a rotation range of 0–270°, with a nominal speed of approximately 315°/s ($\approx$ 53 RPM) at 12.6 V. When coupled with a 20:60 belt transmission ratio, the resulting angular speed at the wrist joint is reduced to approximately 105°/s ($\approx$ 17.5 RPM). Additional mechanical gearing further amplifies torque, enabling the system to surpass the 17 Nm threshold necessary for effective propulsion.

The full electrical scheme is presented in Figure 4.10.

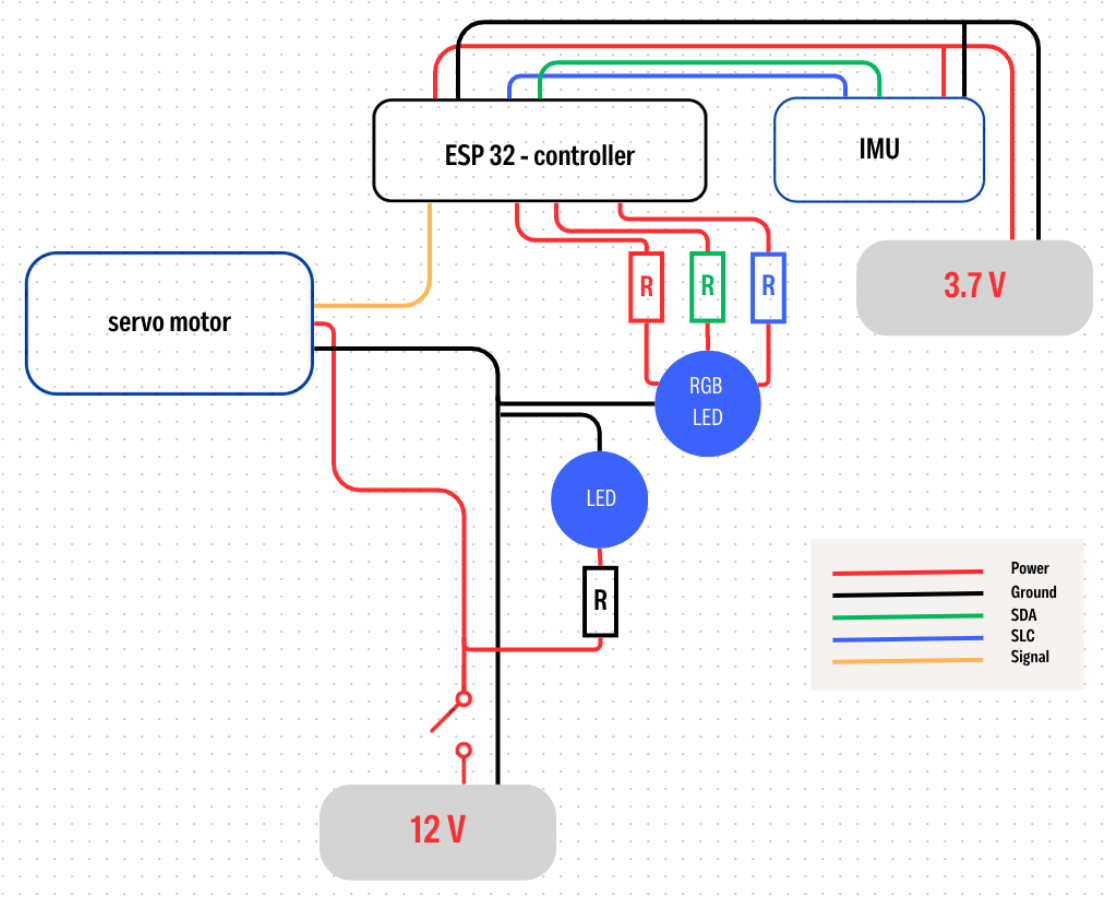


Figure 4.10: Electrical block diagram of the control system.

To power the servo motor, a dedicated high-current power circuit was implemented using a 12 V LiPo battery (Zeee 3S, 1500 mAh, 120C). A blue LED and a 2.2 kΩ resistor were added to indicate power status, and an inline switch was included for immediate shutdown in case of emergency or malfunction.

The controller and IMU are powered separately by a 3.7 V LiPo battery (EEMB, 2000 mAh). The core of the controller is the Adafruit ESP32-S3 Reverse TFT Feather board, selected for its compact form factor, onboard USB-C charging, battery monitoring, support for multiple I^2C peripherals, Wi-Fi and BLE capabilities, and low-power operation that may be beneficial for future upgrades.

For orientation sensing, the Adafruit BNO055 Absolute Orientation Sensor was used. This IMU integrates a 3-axis accelerometer, gyroscope, and magnetometer. This reduces

computational overhead and simplifies real-time control implementation. The IMU communicates with the microcontroller via an I^2C interface using dedicated SDA and SCL lines, which were hardwired (soldered) to the respective I^2C pins on the controller.

An RGB LED with a common anode was also added through a 220 Ω resistor to indicate the battery level of the 3.7 V LiPo battery. The LED operates according to the following logic:

- **Blue:** 100–65% (sufficient for operation)
- **Flashing Red:** 65–55% (battery should be recharged soon)
- **Solid Red:** below 55% (critically low)

Once the circuit was successfully tested and debugged on a breadboard, it was transferred to a solderable prototyping board to improve connection reliability and ensure long-term stability during motion and vibration. The final assembled circuit is shown in Figure 4.11.

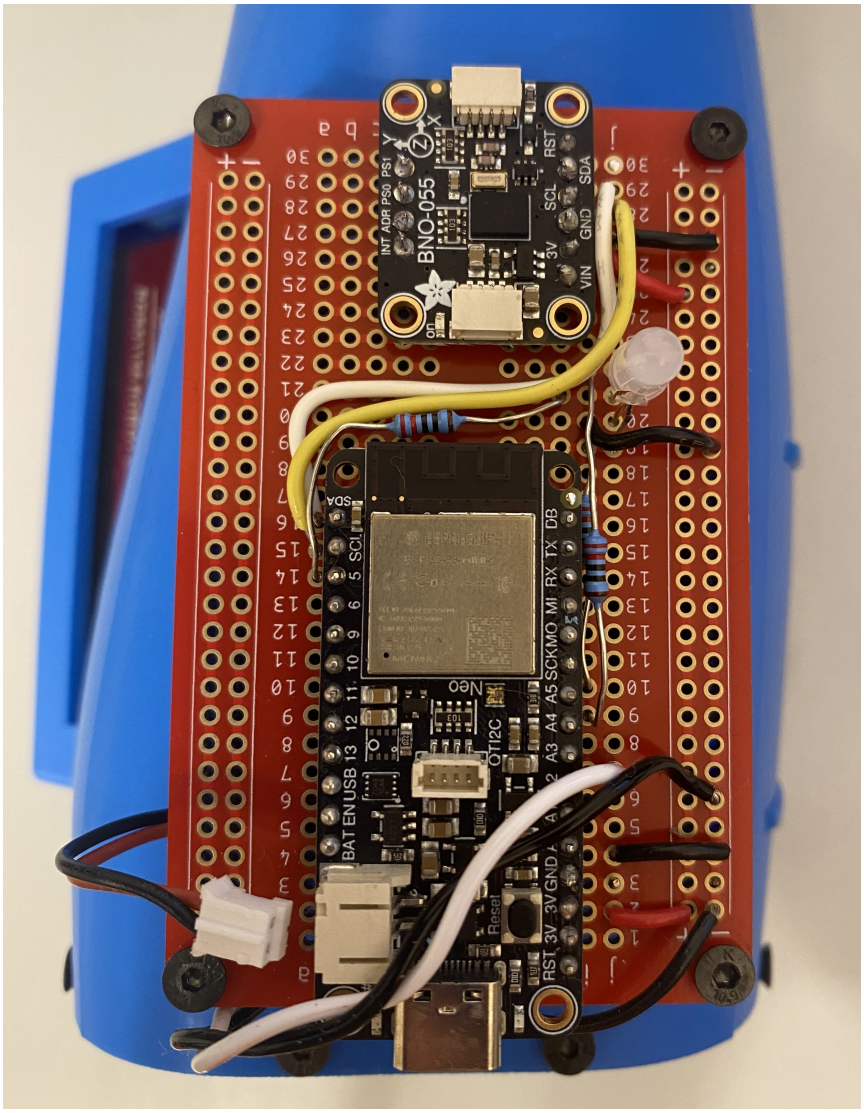


Figure 4.11: Assembled soldered electrical circuit.

Chapter 5

Prototyping

5.1 3D Printing

The main parts of the outer housing were fabricated using a *Bambu Lab P1S* fused filament fabrication 3D printer equipped with a 0.4 mm nozzle. PETG HF filament by Bambu Lab was selected due to its favorable properties for functional prototyping. Compared to PLA, PETG offers improved toughness, better temperature resistance, and reduced brittleness, while still maintaining ease of printing and dimensional stability [57, 58]. Its good resistance to humidity and low warping make it a suitable choice for components exposed to moderate mechanical stress and occasional moisture. However, PETG is not fully waterproof and requires additional sealing treatments for prolonged water submersion, which was not addressed in this prototype stage.

Parts were printed using the manufacturer's standard PETG HF profile on the *Bambu Lab P1S* printer, ensuring reliable results without the need for extensive parameter tuning. The printer's robust capabilities and quality enabled smooth fabrication with minimal issues throughout the process.

Each component was oriented to optimize the layer direction for an effective balance between mechanical strength and surface finish quality. A 20% infill density was applied generally, with increased density in critical load-bearing regions such as screw holes to improve fastening reliability. Support structures were generated for overhangs and complex geometries. To facilitate easy support removal and minimize surface damage, a dedicated interface layer for PLA/PETG was employed. Additionally, brims were added to tall or narrow parts to enhance bed adhesion and prevent warping or detachment during printing.

The wall thickness was consistently set to 5 mm for the majority of components to provide adequate structural integrity while keeping weight manageable. The entire print job consumed approximately 480 g of filament and took about 20 hours to complete, including support structures.

Post-processing involved careful removal of supports and minor surface cleanup to ensure proper fit and assembly. Figure 5.1 illustrates the assembled prototype with multiple views highlighting its range of motion.



Figure 5.1: Prototype: three views illustrating the range of motion.

5.2 Assembling Process

Before physical assembly, all components were virtually assembled in CAD software to validate part compatibility, evaluate mechanical clearances, and determine the optimal sequence of operations. This digital pre-assembly allowed early detection of potential interferences and informed several design refinements, such as repositioning mounting loops and adjusting tolerances. The final CAD model is shown in Figure 5.2.

The assembly process began with attaching the palm-and-fingers unit to the wrist module using perimeter bolts of varying lengths, selected according to load requirements and local geometry constraints. Longer bolts were used in areas with thicker mounting sections to maximize thread engagement, whereas shorter bolts were applied in compact regions to reduce unnecessary weight. Care was taken to ensure that the bolt heads sat as flush as possible with the surface to avoid interference with moving parts. In several locations, complete countersinking was not achieved due to the complex local geometry. This limitation could be resolved in future iterations by adding deeper recesses for bolt heads; however, such changes would require more manual CAD modeling interventions, as they are difficult to implement using only standard automated tools.

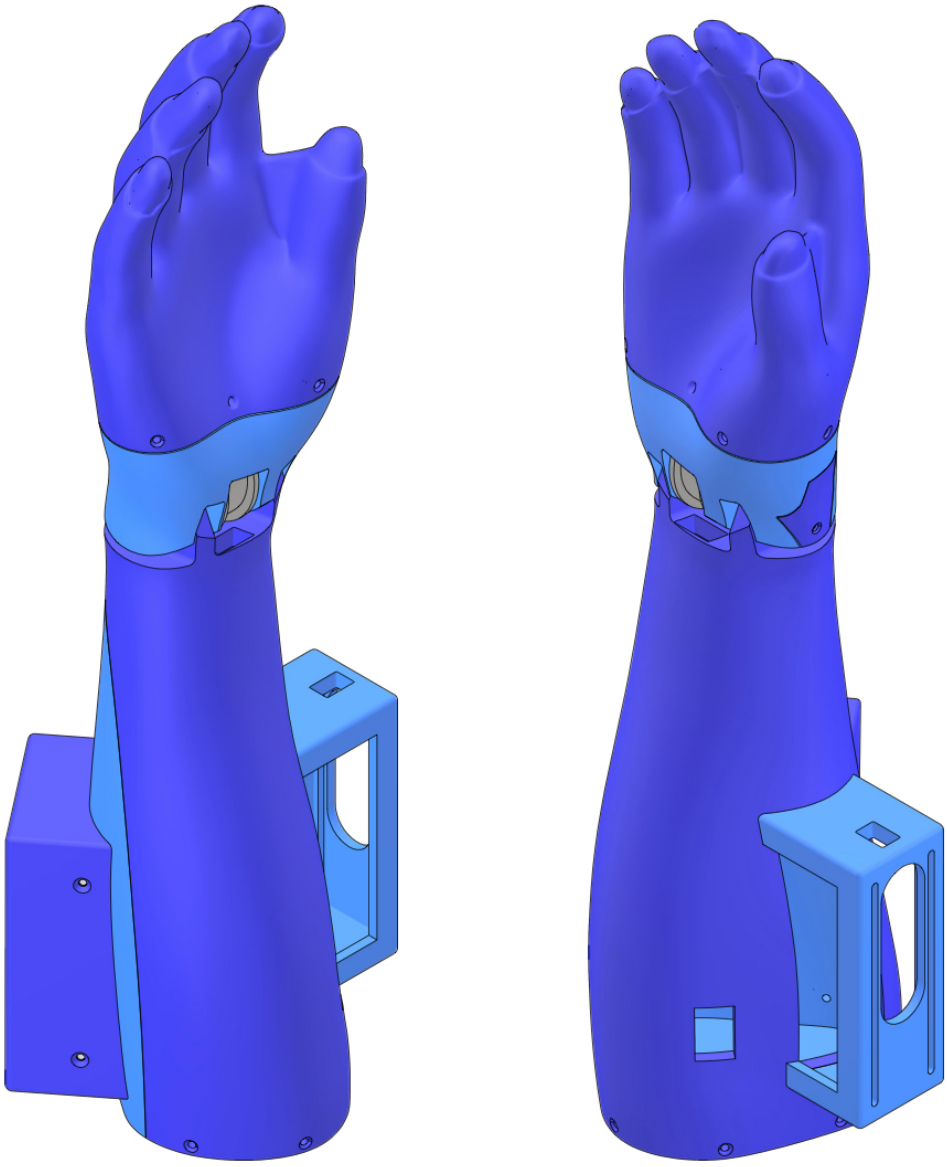


Figure 5.2: Assembled CAD model shown from two perspectives.

A critical early step was securing the central shaft of the wrist mechanism. This component had to satisfy three competing requirements:

1. provide high torsional rigidity under repetitive loading,

2. remain as lightweight as possible, and
3. maintain a compact form factor to avoid adding bulk to the distal section of the prosthesis.

After exploring multiple fixation strategies, a hybrid approach was adopted in which the shaft was locked using a lid pressing onto an M10 hex bolt, achieving both secure retention and minimal play. This method also allowed straightforward disassembly for maintenance.

The mounting loops on the forearm were fitted with custom spacers made from standard steel nuts with the internal threading drilled out. This modification allowed free shaft rotation and ensured metal–metal contact rather than plastic–plastic, improving mechanical durability and reducing tolerance drift over time. Where unavoidable, plastic–plastic contact points were minimized through selective use of washers or metallic inserts.

The pulley, washer, and mounting loops of the wrist mechanism were aligned before the shaft was inserted. Once the mechanism was assembled, the retaining lid was fixed to prevent axial movement of the shaft.

Several additional modifications were made during this stage:

- Four holes were drilled along the side of the forearm to secure the 12V battery with zip ties.
- A feed-through hole was created in the forearm lid to route wires from the servo motor and the 3.7V auxiliary battery.
- A separate aperture was made near the control button to install a 12V battery charge indicator.

The belt-drive system (see Figure 5.3) was implemented using an open belt that was threaded through the designed openings, then glued to form a closed loop. To reinforce the glued joint, a layer of fabric ribbon was wrapped over the seam, enhancing tensile strength under cyclic loading.

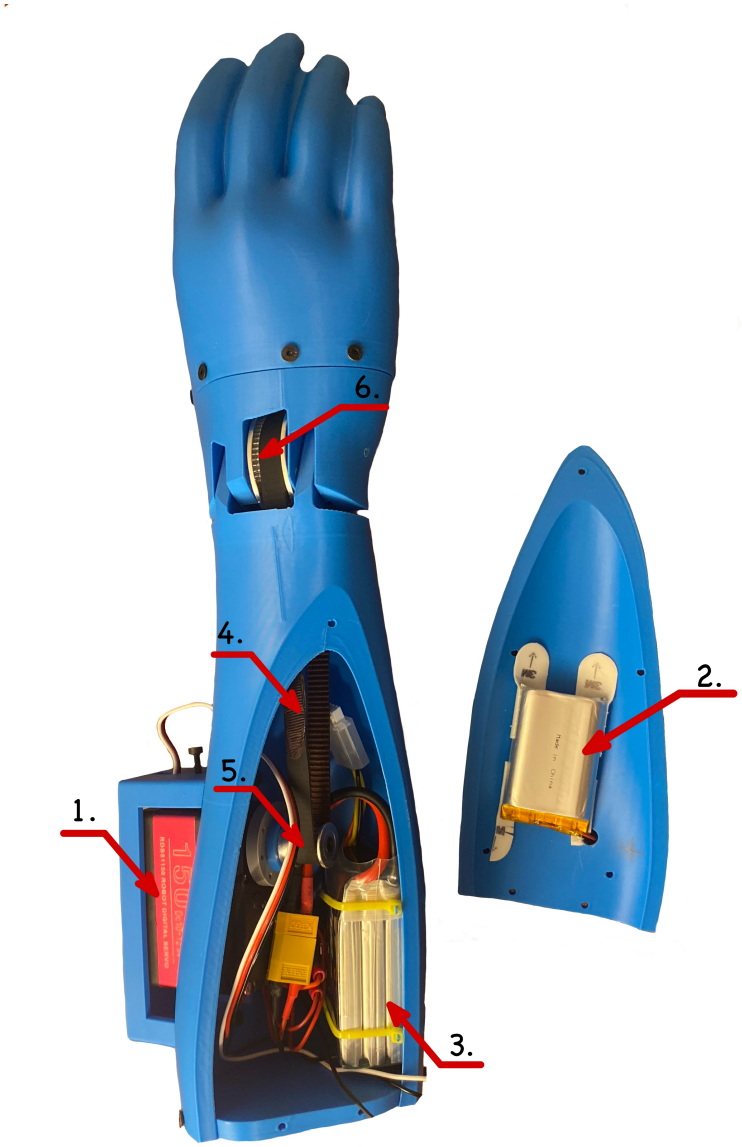


Figure 5.3: Internal view of the prosthesis. Key components are indicated as follows: (1) servo motor, (2) 3.7 V battery, (3) 12 V battery, (4) belt of the belt drive, (5) small pulley, (6) large pulley.

The servo motor bracket and PCB standoffs were mounted to the forearm using stan-

dard bolts. The servo motor was then positioned in its bracket, and its pulley was connected to the belt. Tensioning was achieved via a dedicated mechanism using six bolts, with an additional stabilizing screw to prevent unwanted belt movement during operation. Once optimal belt stability was confirmed, the lower lid of the prosthesis was secured.

Electrical assembly followed mechanical integration. All wiring was routed through the designated openings, with particular attention to preventing abrasion at entry points. The resistor and LED—connected in series after the main switch—were soldered, insulated, and installed into their respective mounts. The 12V battery was placed inside the forearm in a position that avoided interference with the belt path, then fixed using zip ties. The 3.7V battery was attached to the internal side of the forearm lid using high-strength adhesive tape. Wires from this battery were routed through the lid and soldered to the main PCB, which was then secured inside the housing. The assembly was completed by fastening the lid with bolts.

Overall, the assembly process balanced structural integrity, weight minimization, and serviceability. Special emphasis was placed on reducing wear-prone plastic–plastic contact points, optimizing shaft fixation without compromising size or weight, and ensuring that all fastening methods would withstand prolonged mechanical and operational stresses.

5.3 Testing

The final prototype weighs approximately 850 g, which is notably lighter than the average human forearm and hand mass of over 1200 g [59]. While this mass may still be perceived as substantial in air, submerged objects experience buoyant forces that counteract part of their weight. As a result, the prosthesis is expected to feel lighter in water than on land, even without achieving true neutral buoyancy. However, during future testing, it is important to ensure that the buoyancy of the device is close to neutral, as excessive positive buoyancy would require the user to push the prosthesis down with additional effort, while excessive negative buoyancy would require extra force to lift it from the water.

Battery performance was preliminarily evaluated by monitoring voltage drop over a series of short-duration tests under nominal load conditions. Based on these measurements, it is predicted that the servo power supply and microcontroller unit batteries can each support continuous operation for over two hours on a single charge. However, these estimations are limited by the absence of full charge–discharge cycle testing, particularly under realistic aquatic loading conditions where motor demand may vary dynamically. Future work should therefore include comprehensive endurance testing in water, applying realistic

mechanical loads, and monitoring battery life until full discharge to validate operational duration.

Mechanically, the transmission system demonstrated stable output torque and smooth wrist articulation during repeated bench tests, with no observable slippage or overheating. These qualitative observations suggest that the belt-drive and associated components are reliable under the tested conditions, although long-term durability and wear characteristics remain to be assessed.

Kinematic performance of the prosthesis was quantitatively evaluated using digital motion tracking with Tracker [60]. Four anatomical and device-specific landmarks were annotated on the prototype: the distal point of the middle finger, the center of the shaft, and two aligned reference points on the forearm (Figure 5.4). In some frames, points on the prototype were temporarily occluded, and their positions were approximated based on surrounding frames. This annotation provided two-dimensional (X and Y) coordinates of the tracked points across the stroke cycle.

During testing, the prosthesis was held in the tester's hands and rotated to imitate the approximate trajectory of a front crawl stroke. Since only a single limb was used, the recovery phase was naturally reduced, as in real swimming it corresponds to the motion of the contralateral arm.

The recorded trajectories were filtered and segmented into individual strokes. Vectors constructed between the annotated points were then used to calculate wrist flexion–extension angles. A mean stroke profile was generated, and stroke phases were annotated and compared with previously collected dry-land data (Section 3.2).

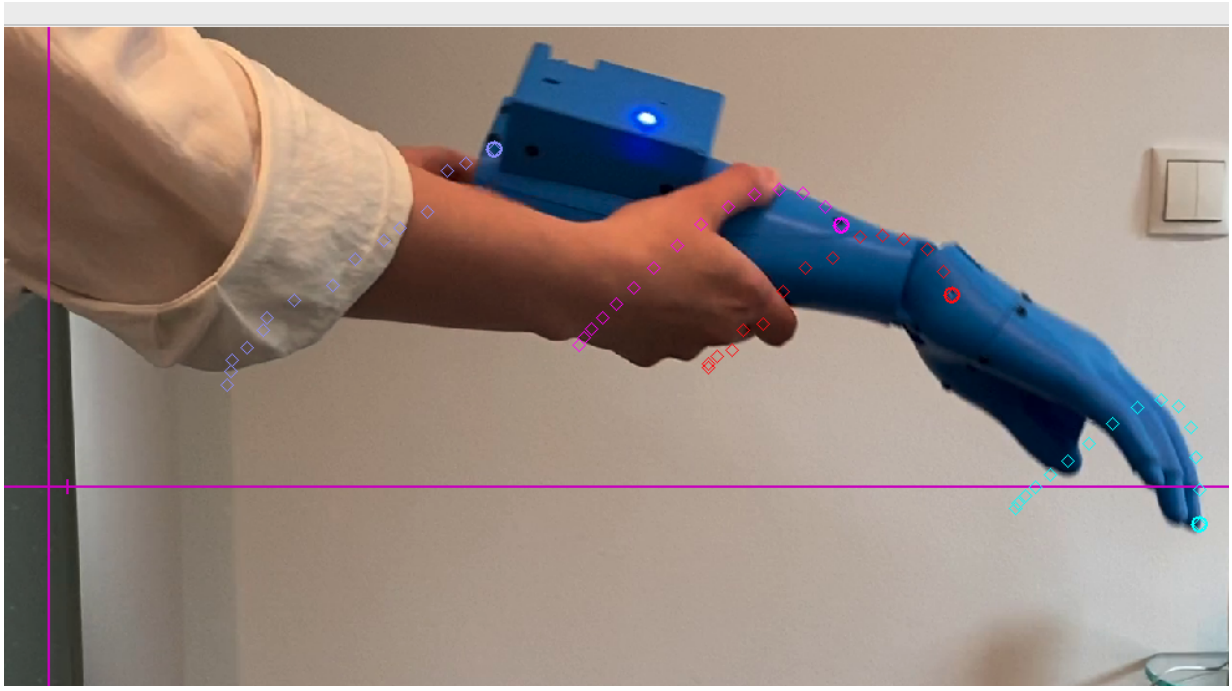


Figure 5.4: Annotated video of the prototype in Tracker, showing magenta axes and four tracked points with their motion traces.

Comparison of the resulting kinematic profiles (Figure 5.5) indicates that the prototype exhibited a wider range of wrist motion (4.5–30°) compared with the dry-land data (15–23°). The standard deviation was also higher for the prototype, likely due to tracking challenges, including occasional point occlusion. Despite these differences, the overall motion trends were consistent across both conditions. Since the control law implements a direct piecewise-linear mapping between ω_{forearm} and wrist angle, the larger range of wrist motion observed in the prototype trials reflects the larger forearm angular velocities recorded during testing.

Stroke phase durations also differed between the two tests. In the dry-land trials, motion was performed more naturally, with symmetrical arm movement extending the recovery phase as the contralateral arm completed its stroke. In contrast, prototype testing relied on a single limb, which made maintaining accurate phase timing more difficult and resulted in shorter stroke phases.

In addition to the mean profiles, the phase portrait of the prototype (Figure 5.6) further illustrates the relationship between forearm angular velocity and wrist angle. The trajectory demonstrates a clear monotonic dependence within each stroke phase, consistent with

the piecewise-linear mapping strategy described in Section 4.3. The annotated phase transition points (catch, pull, push) are aligned along a continuous curve, confirming that the controller switches smoothly between phase-specific mappings. Although the overall range of motion is larger than in the dry-land data, the qualitative shape of the portrait reflects the expected mapping structure (Figure 3.5), supporting the conclusion that the controller responds as intended.

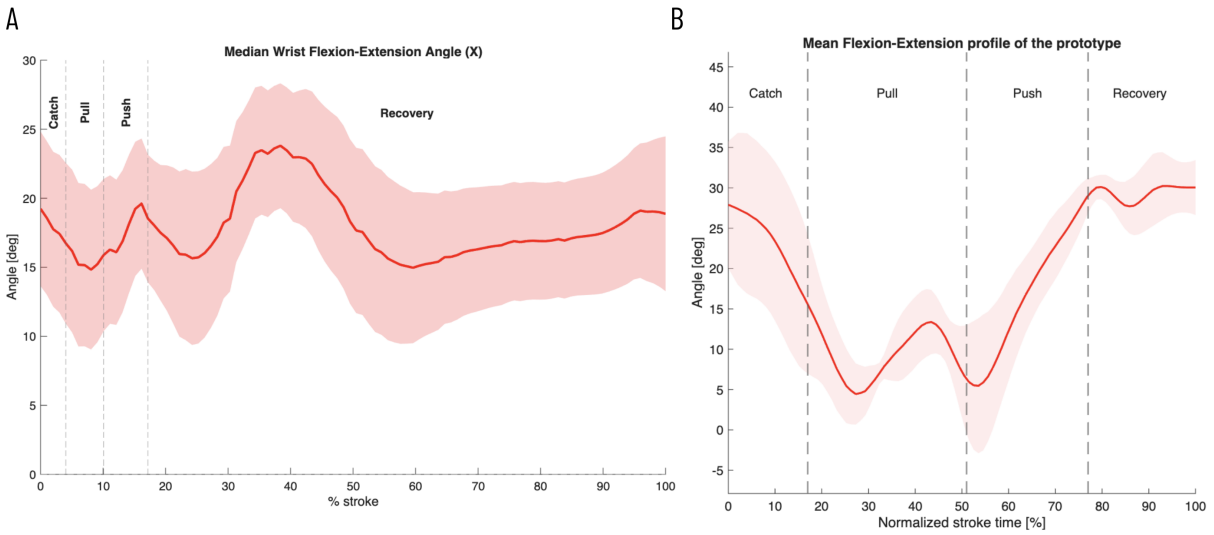


Figure 5.5: Comparison of mean wrist flexion–extension between dry-land trials (Section 3.2) and the prototype: (A) Dry-land motion with labeled stroke phases; shaded area represents ±1 standard deviation. (B) Prototype motion with labeled stroke phases; shaded area represents ±1 standard deviation.

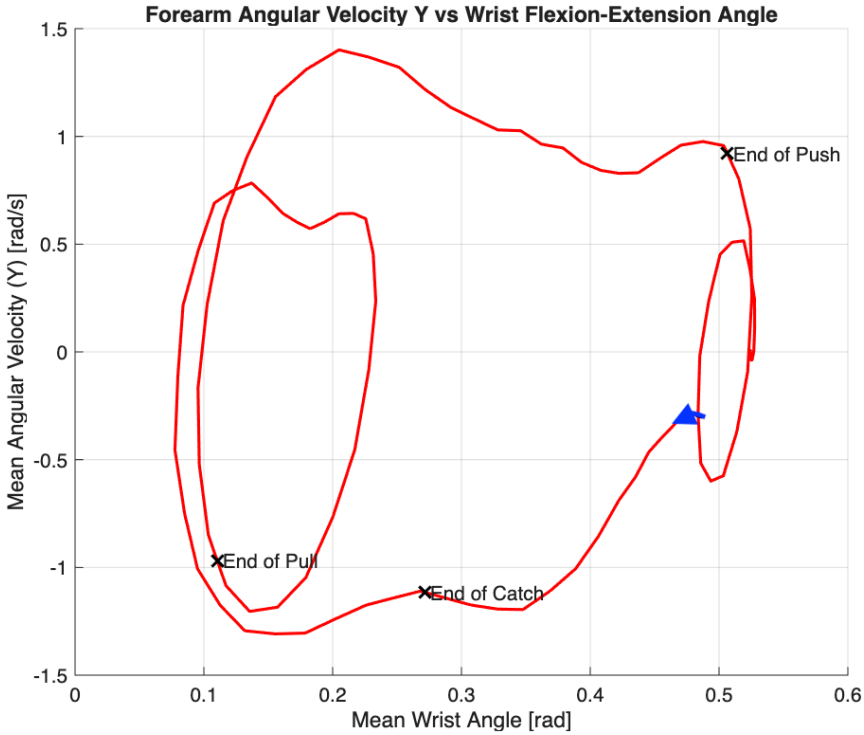


Figure 5.6: Phase portrait of the prosthetic prototype wrist controller: mean forearm angular velocity (Y axis) vs. mean wrist flexion–extension angle (X axis) with annotated stroke phases

Overall, these preliminary tests demonstrate the feasibility of the prototype's design and control approach. Nonetheless, comprehensive aquatic testing involving real users and precise biomechanical measurements is necessary to fully characterize performance, usability, and endurance in swimming environments.

Chapter 6

Conclusions and Future Research

6.1 Contributions

This thesis presents, to the best of the author's knowledge, the first proof-of-concept active upper-limb prosthesis specifically designed for swimming. Unlike existing passive solutions, the proposed prototype actively adapts wrist orientation in real time according to the swimming stroke phase. This approach aims to enhance propulsion symmetry, reduce compensatory movements, and support rehabilitation for upper-limb amputees in aquatic environments.

The key contributions of this work are as follows:

- Analyzed front crawl swimming kinematics with a focus on wrist motion patterns across different stroke phases.
- Developed a novel biomechanically-informed control strategy for phase-based wrist adaptation using IMU data.
- Designed and fabricated a mechanical structure replicating the human hand's hydrodynamic form, enabling one DOF in wrist rotation.
- Applied a hybrid modeling workflow (polygonal and CAD-based) to capture anatomical geometry while ensuring manufacturability via 3D printing.

Overall, this thesis establishes a foundation for future research into adaptive, low-cost, and sport-oriented prosthetic solutions that extend upper-limb functionality into aquatic

environments, with potential applications in both competitive swimming and rehabilitation.

6.2 Limitations

While the prototype demonstrates the feasibility of an active, swimming-oriented upper-limb prosthesis, several design and implementation constraints currently limit its practical deployment. Addressing these issues will be essential for translating the concept into a reliable, user-ready device.

One major constraint lies in the size and arrangement of the electronic components, which restrict the overall compactness of the prosthesis. This limitation hinders the integration of a fully enclosed housing, a prerequisite for effective waterproofing. Future iterations could benefit from miniaturized or custom-designed electronics, though such approaches may increase production costs, especially for individualized manufacturing.

The actuation system also presents potential reliability challenges. The current belt-drive transmission requires consistent tension to maintain performance, yet belts can loosen or slip under load, reducing effective torque transfer to the wrist. Such losses could compromise propulsion and swimming symmetry. Replacing the belt drive with alternative transmission methods, such as a compact gear train or a direct-drive motor, could improve torque transfer efficiency, enhance durability, and reducing maintenance needs.

Material choice and manufacturing methods further influence device longevity. While 3D printing offers rapid prototyping and anatomical customization, certain printed materials may lack the fatigue resistance needed for prolonged use in aquatic conditions. Exploring lightweight, high-strength alternatives, for instance carbon fiber composites or advanced engineering polymers, could enhance both durability and user comfort.

The most critical limitation is the absence of waterproofing, which currently prevents real-world aquatic trials. Without adequate sealing, both device integrity and user safety are at risk. Potential solutions include encapsulating the prosthesis within a custom silicone glove, complemented by conformal waterproof coatings for the electronics. Such measures would be a prerequisite for safe in-water testing and long-term deployment.

Another important part of the device is the socket that attaches the prosthesis to the residual limb. Although this component was not the focus of the present work, proper socket fitting is crucial for both comfort and functionality. In swimming applications, the socket may need to be tighter than in everyday use to prevent unwanted movement.

Additional attachment methods, such as Velcro straps, could be required. If the socket is too loose, it could lead to undesired rotation or even detachment of the prosthesis during use.

From a control standpoint, the current implementation based on threshold detection has inherent limitations. Thresholds tuned to one swimmer or one set of conditions may not generalize well to variations in pace, stroke technique, or fatigue, which could compromise reliability in real-world use. In future iterations, more adaptive approaches could be explored. For instance, integrating machine learning methods could allow the system to recognize stroke patterns from the initial trajectory and dynamically adjust the wrist angle throughout the cycle. Moreover, incorporating wireless connectivity, such as Bluetooth, would not only enable real-time data logging for performance analysis and refinement but also facilitate remote calibration and updates. These enhancements would help overcome the rigidity of the threshold-based method and improve both robustness and user experience in diverse swimming scenarios.

By systematically addressing these limitations, future versions of the device could progress from a laboratory proof-of-concept toward a robust, field-ready solution capable of meeting the functional and environmental demands of swimming.

6.3 Opportunities for Future Work

The current prototype establishes the feasibility of phase-based control for wrist flexion in a swimming prosthesis, yet substantial refinements are necessary before transitioning toward a deployable, user-ready product. Future work can be broadly categorized into control development, sensing enhancement, mechanical optimization, and application expansion.

From a control perspective, further research should prioritize the collection of kinematic data from swimmers with varying skill levels, swimming techniques, and physical conditions. A more diverse dataset would enable the development of control strategies that are both robust and generalizable. Additionally, incorporating machine learning algorithms trained on larger datasets could improve the controller's adaptability, allowing it to respond dynamically to changes in pace, fatigue, or stroke variability. Examining stroke symmetry should also be a priority, as restoring or promoting bilateral coordination is a central goal of prosthetic swimming applications.

Enhancing sensing capabilities represents another key opportunity. Supplementary IMUs positioned on the contralateral wrist—potentially embedded in a smartwatch—or

mounted on swimming goggles could provide complementary motion data. Such multi-sensor integration may improve stroke phase detection accuracy and enable the controller to adapt more effectively to individual swimming styles.

The implementation of a user-specific calibration procedure would allow the prosthesis to be tuned to individual biomechanics and personal preferences, thereby improving both comfort and performance. Introducing a dedicated user interface, whether as a mobile application or a physical control panel, could facilitate calibration, mode switching, and performance monitoring in real time.

Mechanical improvements could include adding an additional degree of freedom, such as wrist pronation/supination, to optimize the angle of attack during the stroke and potentially enhance propulsion. Developing an ergonomic and secure socket tailored to the residual limb is equally essential, as comfort and stability are prerequisites for long-term adoption.

Expanding the control framework to accommodate additional swimming strokes—such as breaststroke, backstroke, and butterfly—offers another promising direction. While the phase-based approach may remain conceptually applicable, each stroke will require dedicated kinematic modeling and possibly significant modifications to both the mechanical design and control architecture.

Lastly, the underlying methodology could be adapted for a wider range of disabilities and limb differences — for example, higher-level limb amputations or assistive devices for individuals with muscle or neurological impairments that limit natural swimming motions. Such applications would require more substantial modifications to the prosthesis design, but could further broaden the inclusivity and societal impact of adaptive swimming technologies. Such extensions would position the technology not only as a rehabilitation tool but also as a means of enabling active participation in aquatic sports for diverse user groups.

References

[1] Steeper Group. Trs water sports and activity terminal devices, n.d. Accessed: 2025-08-08.

[2] G. P. Millet, D. Chollet, S. Chalies, and J. C. Chatard. Coordination in front crawl in elite triathletes and elite swimmers. *International Journal of Sports Medicine*, 23(2):99–104, February 2002.

[3] Amir Hesami, Fazel Naghdy, David Stirling, and Harold Hill. Application of Fuzzy NARX to Human Gait Modelling and Identification. In *ResearchGate*, January 2008.

[4] Chad A. Krueger, Joseph C. Wenke, and James R. Ficke. Ten years at war: Comprehensive analysis of amputation trends. *Journal of Trauma and Acute Care Surgery*, 73(6):S438, December 2012.

[5] Lynn G. Stansbury, Steven J. Lalliss, Joanna G. Branstetter, Mark R. Bagg, and John B. Holcomb. Amputations in U.S. Military Personnel in the Current Conflicts in Afghanistan and Iraq. *Journal of Orthopaedic Trauma*, 22(1):43, January 2008.

[6] Asma Salari and Seyed Hossein Hosseini. Russia's Attack on Ukraine: A Review of the International Criminal Court's Capacity to Examine the Crime of Aggression. *Access to Justice in Eastern Europe*, 2023(1):8–27, 2023.

[7] Yordan Gunawan and Mhd. Ervizal Rizqy Pane. Responsibility for Excessive Infrastructure Damage in Attacks: Analysing Russia's Attack in Ukraine. *PETITA: Jurnal Kajian Ilmu Hukum dan Syariah (PJKIHdS)*, 9(1):212–231, 2024.

[8] P.S. Mckechnie and A. John. Anxiety and depression following traumatic limb amputation: A systematic review. *Injury*, 45(12):1859–1866, December 2014.

[9] Germain Pomares, Henry Coudane, François Dap, and Gilles Dautel. Traumatic upper-limb amputation: The process toward acceptance. *Orthopaedics & Traumatology: Surgery & Research*, 106(7):1419–1423, November 2020.

[10] Samuel Cohen-Tanugi, Risa Reid, Bryan J. Loeffler, and R. Glenn Gaston. The Prevalence of Depression and PTSD in Adults With Surgically Managed Traumatic Upper-Extremity Amputations. *Hand (New York, N.Y.)*, 19(1):169–174, January 2024.

[11] Xaver Fuchs, Herta Flor, and Robin Bekrater-Bodmann. Psychological Factors Associated with Phantom Limb Pain: A Review of Recent Findings. *Pain Research & Management*, 2018:5080123, June 2018.

[12] Carly S. Eckard, Alison L. Pruziner, ATC, Allison D. Sanchez, and Anne M. Andrews. Metabolic and body composition changes in first year following traumatic amputation. *Journal of Rehabilitation Research and Development*, 52(5):553–562, 2015.

[13] Ian M. Lahart and George S. Metsios. Chronic Physiological Effects of Swim Training Interventions in Non-Elite Swimmers: A Systematic Review and Meta-Analysis. *Sports Medicine (Auckland, N.Z.)*, 48(2):337–359, February 2018.

[14] Motomu Nakashima and Yohei Chida. Effects of paddle dimensions on shoulder joint torque for a swimmer with unilateral transradial deficiency. *Sports Engineering*, 26(1):1, December 2022.

[15] Bryce TJ Dyer and Sarah A Deans. Swimming with limb absence: A systematic review. *Journal of Rehabilitation and Assistive Technologies Engineering*, 4:2055668317725451, August 2017.

[16] N. S. Schreiber and R. T. T. Gettens. Aquatic design for individuals with disabilities: Upper limb prosthesis. In *2014 40th Annual Northeast Bioengineering Conference (NEBEC)*, pages 1–2, April 2014. ISSN: 2160-7028.

[17] M. A. Lauder and P. Dabnichki. Estimating propulsive forces—sink or swim? *Journal of Biomechanics*, 38(10):1984–1990, October 2005.

[18] International Paralympic Committee. Paralympic games – news, sports and results, 2025. Accessed: 3 August 2025.

[19] G. Pomares, H. Coudane, F. Dap, and G. Dautel. Epidemiology of traumatic upper limb amputations. *Orthopaedics & Traumatology: Surgery & Research*, 104(2):273–276, April 2018.

[20] Germain Pomares, Henry Coudane, François Dap, and Gilles Dautel. Psychological effects of traumatic upper-limb amputations. *Orthopaedics & Traumatology: Surgery & Research*, 106(2):297–300, April 2020.

[21] Mitchell A. Pet, Shane D. Morrison, Jacob S. Mack, Erika D. Sears, Thomas Wright, Alisha D. Lussiez, Kenneth R. Means, James P. Higgins, Jason H. Ko, Paul S. Cederna, and Theodore A. Kung. Comparison of patient-reported outcomes after traumatic upper extremity amputation: Replantation versus prosthetic rehabilitation. *Injury*, 47(12):2783–2788, December 2016.

[22] Peter Fitzgibbons and Gleb Medvedev. Functional and Clinical Outcomes of Upper Extremity Amputation. *JAAOS - Journal of the American Academy of Orthopaedic Surgeons*, 23(12):751, December 2015.

[23] C. L. Semasinghe, J. L. B. Prasanna, H. M. Kandamby, R. K. P. S. Ranaweera, D. G. K. Madusanka, and R. A. R. C. Gopura. Transradial prostheses: Current status and future directions. In *2016 Manufacturing & Industrial Engineering Symposium (MIES)*, pages 1–7, October 2016.

[24] Wen Xu, Yoshiko Toyoda, and Ines C. Lin. Upper Extremity Prosthetics: Current Options and Future Innovations. *Journal of Hand Surgery*, 48(10):1034–1044, October 2023. Publisher: Elsevier.

[25] Kai Xu and Sheng-Feng Qin. 3D Printing, Limb Prosthetics and Generative Design: A Scoping Review. In *2022 27th International Conference on Automation and Computing (ICAC)*, pages 1–6, September 2022.

[26] S. Vijay Ananth, Ayush Patawari, K. Sundari, Raghavi, Likitha, and S. Arivalagan. Biomechanical Sports Analysis Using Inertial Measurement Unit. In *2019 IEEE International Conference on System, Computation, Automation and Networking (ICSCAN)*, pages 1–5, March 2019.

[27] Yansong Wang, Xu Cheng, Leen Jabban, Xiaohong Sui, and Dingguo Zhang. Motion Intention Prediction and Joint Trajectories Generation Toward Lower Limb Prostheses Using EMG and IMU Signals. *IEEE Sensors Journal*, 22(11):10719–10729, June 2022. Conference Name: IEEE Sensors Journal.

[28] Agamemnon Krasoulis, Sethu Vijayakumar, and Kianoush Nazarpour. Multi-Grip Classification-Based Prosthesis Control With Two EMG-IMU Sensors. *IEEE transactions on neural systems and rehabilitation engineering: a publication of the IEEE Engineering in Medicine and Biology Society*, 28(2):508–518, February 2020.

[29] Honglei Zhang, Sidi Mohamed Sid'El Moctar, Sofiane Boudaoud, and Imad Rida. A comprehensive review of sEMG-IMU sensor fusion for upper limb movements pattern recognition. *Information Fusion*, 125:103422, January 2026.

[30] Srikanth Sagar Bangaru, Chao Wang, and Fereydoun Aghazadeh. Data Quality and Reliability Assessment of Wearable EMG and IMU Sensor for Construction Activity Recognition. *Sensors (Basel, Switzerland)*, 20(18):5264, September 2020.

[31] Daniel A. Bennett and Michael Goldfarb. IMU-Based Wrist Rotation Control of a Transradial Myoelectric Prosthesis. *IEEE Transactions on Neural Systems and Rehabilitation Engineering*, 26(2):419–427, February 2018.

[32] Riccardo Galviati, Nicolò Boccardo, Michele Canepa, Dario Di Domenico, Andrea Marinelli, Carlo Albino Frigo, Matteo Laffranchi, and Lorenzo De Michieli. IMU Sensors Measurements Towards the Development of Novel Prosthetic Arm Control Strategies. In *2023 International Conference on Rehabilitation Robotics (ICORR)*, pages 1–6, Singapore, Singapore, September 2023. IEEE.

[33] Morgan Jackson, Manjot Kang, James Furness, and Kevin Kemp-Smith. Aquatic exercise and mental health: A scoping review. 2022.

[34] Effects of aquatic exercise on mood and anxiety symptoms: A systematic review and meta-analysis - PubMed.

[35] K. Overbury, B. W. Conroy, and E. Marks. Swimming in nature: A scoping review of the mental health and wellbeing benefits of open water swimming. *Journal of Environmental Psychology*, 90:102073, September 2023.

[36] Raul F. Bartolomeu, Mário J. Costa, and Tiago M. Barbosa. Contribution of limbs' actions to the four competitive swimming strokes: a nonlinear approach. *Journal of Sports Sciences*, 36(16):1836–1845, August 2018. Publisher: Routledge _eprint: https://doi.org/10.1080/02640414.2018.1423608.

[37] V. J. Deschodt, L. M. Arsac, and A. H. Rouard. Relative contribution of arms and legs in humans to propulsion in 25-m sprint front-crawl swimming. *European Journal of Applied Physiology and Occupational Physiology*, 80(3):192–199, July 1999.

[38] Mathias Samson, Anthony Bernard, Tony Monnet, Patrick Lacouture, and Laurent David. Unsteady computational fluid dynamics in front crawl swimming. *Computer Methods in Biomechanics and Biomedical Engineering*, 20(7):783–793, May 2017. Publisher: Taylor & Francis.

[39] Ross H. Sanders, Jordan T. Andersen, and Hideki Takagi. The Segmental Movements in Front Crawl Swimming. In Bertram Müller, Sebastian I. Wolf, Gert-Peter Brueggemann, Zhigang Deng, Andrew McIntosh, Freeman Miller, and William Scott Selbie, editors, *Handbook of Human Motion*, pages 1–15. Springer International Publishing, Cham, 2017.

[40] Simon Harrison, Raymond Cohen, Paul Cleary, Bruce Mason, and David Pease. Torque and power about the joints of the arm during the freestyle stroke. January 2014.

[41] Jiaxin Wang, Zhelong Wang, Fengshan Gao, Hongyu Zhao, Sen Qiu, and Jie Li. Swimming Stroke Phase Segmentation Based on Wearable Motion Capture Technique. *IEEE Transactions on Instrumentation and Measurement*, 69(10):8526–8538, October 2020. Conference Name: IEEE Transactions on Instrumentation and Measurement.

[42] Mohamed Amin Regaieg, Adrien J. Létocart, Jérôme Bosche, Ludovic Seifert, and Brice Guignard. Automatic Detection of Key Points of the Cycle to Assess Upper Limb Coordination in Front Crawl: Effect of Swimming Speed and Impairment. *IEEE Sensors Journal*, 23(16):17979–17989, August 2023. Conference Name: IEEE Sensors Journal.

[43] Julien Pansiot, Benny Lo, and Guang-Zhong Yang. Swimming Stroke Kinematic Analysis with BSN. In *2010 International Conference on Body Sensor Networks*, pages 153–158, June 2010. ISSN: 2376-8894.

[44] Matteo Cortesi, Rocco Di Michele, Silvia Fantozzi, Sandro Bartolomei, and Giorgio Gatta. Arm-Stroke Descriptor Variability during 200-m Front Crawl Swimming. *Sensors (Basel, Switzerland)*, 21(2):324, January 2021.

[45] Hideki Takagi, Motomu Nakashima, Yasuo Sengoku, Takaaki Tsunokawa, Daiki Koga, Kenzo Narita, Shigetada Kudo, Ross Sanders, and Tomohiro Gonjo. How do swimmers control their front crawl swimming velocity? Current knowledge and gaps from hydrodynamic perspectives. *Sports Biomechanics*, 22(12):1552–1571, December 2023. Publisher: Routledge _eprint: https://doi.org/10.1080/14763141.2021.1959946.

[46] Stefan Salminger, Heiko Stino, Lukas H. Pichler, Clemens Gstoettner, Agnes Sturma, Johannes A. Mayer, Michael Szivak, and Oskar C. Aszmann. Current rates of prosthetic usage in upper-limb amputees - have innovations had an impact on device acceptance? *Disability and Rehabilitation*, 44(14):3708–3713, July 2022.

[47] John R. Fredieu, Jennifer Kerbo, Mark Herron, Ryan Klatte, and Malcolm Cooke. Anatomical Models: a Digital Revolution. *Medical Science Educator*, 25(2):183–194, June 2015.

[48] Neculai Archip, Robert Rohling, Vincent Dessenne, Pierre-Jean Erard, and Lutz Peter Nolte. Anatomical structure modeling from medical images. *Computer Methods and Programs in Biomedicine*, 82(3):203–215, June 2006.

[49] Nikola Vukašinović and Jože Duhovnik. *Advanced CAD Modeling | springerprofessional.de*. Springer, 2019.

[50] Mario Russo. *Polygonal Modeling: Basic and Advanced Techniques*. Jones & Bartlett Learning, 2006.

[51] Taehyun Rhee, Ulrich Neumann, and J. P. Lewis. Human hand modeling from surface anatomy. In *Proceedings of the 2006 symposium on Interactive 3D graphics and games - SI3D '06*, page 27, Redwood City, California, 2006. ACM Press.

[52] C. López, J. A. Peña, and R. Miralbés. 3D Organic Modeling Using Hybrid Techniques with Polygons. In Francisco Cavas-Martínez, Benoit Eynard, Francisco J. Fernández Cañavate, Daniel G. Fernández-Pacheco, Paz Morer, and Vincenzo Nigrelli, editors, *Advances on Mechanics, Design Engineering and Manufacturing II*, pages 263–271, Cham, 2019. Springer International Publishing.

[53] KoasterDude195 (Eli). Polygonal 3d hand model. Shared on Discord channel where artists share models for public use, 2025. Accessed July 2025; personal communication.

[54] Cheryl D. Fryar, Margaret D. Carroll, Qiuping Gu, Joseph Afful, and Cynthia L. Ogden. Anthropometric reference data for children and adults : United States, 2015-2018.

[55] Kyle Casadei and John Kiel. Anthropometric Measurement. In *StatPearls*. StatPearls Publishing, Treasure Island (FL), 2025.

[56] Joris van den Berg, Rens Bazuin, Constantin Jux, Andrea Sciacchitano, Jerry Westerweel, and Willem van de Water. The effect of hand posture on swimming efficiency. *Experiments in Fluids*, 62(12):245, November 2021.

[57] Ksawery Szykiedans, Wojciech Credo, and Dymitr Osiński. Selected Mechanical Properties of PETG 3-D Prints. *Procedia Engineering*, 177:455–461, 2017.

[58] Arda Özen, Bilen Emek Abali, Christina Völlmecke, Jonathan Gerstel, and Dietmar Auhl. Exploring the Role of Manufacturing Parameters on Microstructure and Mechanical Properties in Fused Deposition Modeling (FDM) Using PETG. *Applied Composite Materials*, 28(6):1799–1828, December 2021.

[59] Wilfrid Taylor Dempster and George R. L. Gaughran. Properties of body segments based on size and weight. *American Journal of Anatomy*, 120(1):33–54, 1967. _eprint: https://anatomypubs.onlinelibrary.wiley.com/doi/pdf/10.1002/aja.1001200104.

[60] Douglas Brown. Tracker video analysis and modeling tool. Available at: https://physlets.org/tracker/, 2023. Open Source Physics project.

APPENDICES

Appendix A

Bill of Materials (BOM) for the swimming prosthesis prototype

The table below summarizes the core hardware components used in the development of the prosthetic prototype. It includes specifications relevant to functionality and integration, as well as indicative brands and price estimates where applicable. These components were selected based on requirements for waterproofing, energy efficiency, real-time processing, and compatibility with 3D-printed enclosures.

Table A.1: List of hardware components used in the prosthetic prototype

Component	**Specification**	**Price (CAD)**
Servo motor	150 kg.cm torque, 12V, 270° rotation	59
ESP32 microcontroller (Adafruit)	Wi-Fi + BLE enabled	24.95
IMU BNO055 (Bosch)	9 DOF, onboard fusion algorithm	29.95
Synchronous wheel G2	20×60 mm, 11 mm belt width	26
Timing belt G2	9 mm width, 2 m length, 2 mm teeth pitch	11
LiPo battery (motor)	3S, 1500 mAh, 12V	46
LiPo battery (IMU/controller)	3.7V, 1000 mAh	25
Solderable boards (generic)	Set of 3 boards	14
Resistor kit	Assorted, 0 Ω – 1 MΩ	16
LED kit	Standard assorted types	16
Screw kit	460 pcs, M3 sizes	16